

Constraining the onset of orogenic contraction in fold-and-thrust belts using sedimentary stylolite populations (Umbria-Marche Apennines, Italy)

Aurélie Labeur^a, Nicolas E. Beaudoin^{a,*}, Olivier Lacombe^b, Claude Gout^a, Jean-Paul Callot^a

^a Université de Pau et des Pays de L'Adour, LFCR, E2S-UPPA, CNRS, Pau, France

^b Sorbonne Université, CNRS-INSU, Institut des Sciences de La Terre de Paris - ISTEP, Paris, France

ARTICLE INFO

Keywords:

Paleopiezometry
Stylolites
Signal processing
Paleodepth
Layer parallel shortening
Fold-and-thrust belts

ABSTRACT

Stylolites are pressure solution structures, the roughness of which yields quantitative information about the magnitude of the normal stress applied to the stylolite plane. The stress magnitude is calculated from the cross over length (L_c) determined using the signal analysis of a 2D track. For a sedimentary, bedding-parallel stylolite (BPS), L_c scales to the magnitude of the vertical maximum principal stress σ_1 , hence to the burial depth at the time the roughness of the stylolite froze. We present a dataset of nearly 200 BPS from Meso-Cenozoic folded carbonates across the Umbria Marche Apennine Ridge. The BPS population is used to address the discrepancies between L_c values obtained by using different signal analysis methods. Assuming that in compressional settings burial-related pressure-solution more probably halts because of the switch of σ_1 from a burial-related vertical attitude to a tectonic-related horizontal attitude, the vertical stress magnitudes derived from the inversion of the BPS roughness were combined to burial models at each investigated fold to reconstruct the absolute timing at which the orogenic stress started to prevail. The results indicate that the onset of horizontal compression started at ~ 10 Ma and ~ 8 Ma in the innermost and outermost folds, respectively, and predated fold development as indicated by the age of growth strata. These results establish Stylolite Roughness Inversion Technique as a reliable depth gauge that enables refining the timing of the onset of contraction in fold-and-thrust belts.

1. Introduction

Sedimentary stylolites are pressure-solution surfaces frequently observed in sedimentary rocks, and usually developed parallel to bedding in sub-horizontal strata during burial, *i.e.* when the state of stress was dominated by the burial stress, so that the maximum principal stress σ_1 was vertical (Stockdale, 1926; Alvarez et al., 1978; Koehn et al., 2007; Ebner et al., 2009b; Ben-Itzhak et al., 2012; Toussaint et al., 2018). They are characterized by physical properties such as amplitude, morphology and roughness (Fig. 1A). The 1D roughness of the track of a stylolite, defined as the difference in height between two points separated by a set distance along the track, yields 2 self-affine regimes according to the scale of observation (Renard et al., 2004; Schmittbuhl et al., 2004). This is the base of the use of the roughness of stylolites as a paleopiezometer, *i.e.* the so-called Stylolite Roughness Inversion Technique (SRIT). SRIT is a recently developed approach that enables the quantification of the magnitude of the vertical stress when applied to sedimentary stylolites (Schmittbuhl et al., 2004). The underlying stylolite growth model (Koehn et al., 2007; Ebner et al., 2009a; Rolland

et al., 2012; Toussaint et al., 2018) discriminates two main scaling regimes depending on the predominant energy, each regime being characterized by a power law governed by a specific roughness exponent (*i.e.*, Hurst exponent) in the signal analysis spectrum (Fig. 1B): (i) the surface energy-controlled scale, characterized by a steep slope and a roughness exponent of 1.1 ± 0.1 , and (ii) the elastic energy-controlled scale, associated with a gentle slope and a Hurst exponent between 0.5 and 0.6 (Barabási and Stanley, 1995; Renard et al., 2004; Schmittbuhl et al., 2004). The spatial scale at which there is a transition between these two regimes, the so-called crossover length L_c , is directly related to the magnitude of prevalent mean and differential stresses in the strata at the time the stylolite stopped to be an active dissolution surface.

Meanwhile the whereabouts of stylolite roughness evolution and fossilization were further investigated (Ebner et al., 2009a; Koehn et al., 2012, 2022; Rolland et al., 2012), SRIT has been applied to populations of bedding-parallel (sedimentary) stylolites (BPS hereinafter) in order to predict the maximum burial depth at which σ_1 was still vertical (e.g. Beaudoin et al., 2016, 2019, 2020c; b; Bertotti et al., 2017; Labeur et al., 2021; Lacombe et al., 2021; Bah et al., 2023; Zeboudj et al., 2023). That

* Corresponding author: Batiment IPRA, LFCR, Avenue de l'université, 64000 Pau, France.

E-mail address: nicolas.beaudoin@univ-pau.fr (N.E. Beaudoin).

<https://doi.org/10.1016/j.jsg.2024.105098>

Received 6 November 2023; Received in revised form 23 January 2024; Accepted 7 March 2024

Available online 24 March 2024

0191-8141/© 2024 The Authors. Published by Elsevier Ltd. This is an open access article under the CC BY license (<http://creativecommons.org/licenses/by/4.0/>).

property was used in relatively undeformed sedimentary basins (Ebner et al., 2009b; Beaudoin et al., 2019), at passive margins (Bah et al., 2023; Zeboudj et al., 2023) or in foreland basins (Beaudoin et al., 2016, 2020c; Bertotti et al., 2017; Labeur et al., 2021). In most cases, the combination of the reconstructed burial depth experienced during stylolite development with the burial-time evolution of the strata hosting the stylolites provided valuable time constraints on the burial and

tectonic history (Fig. 1C), as well as new insights into the impact of fold type and tectonic style on the timing and sequence of contractional deformation in fold-and-thrust belts (e.g., Lacombe et al., 2021). Through such case studies, the quantitative results returned by SRIT (i.e. the magnitude of the vertical stress, converted into burial depth), although limited to the maximum depth recorded by the deepest stylolites developed during burial, are very impactful. SRIT then stands as a

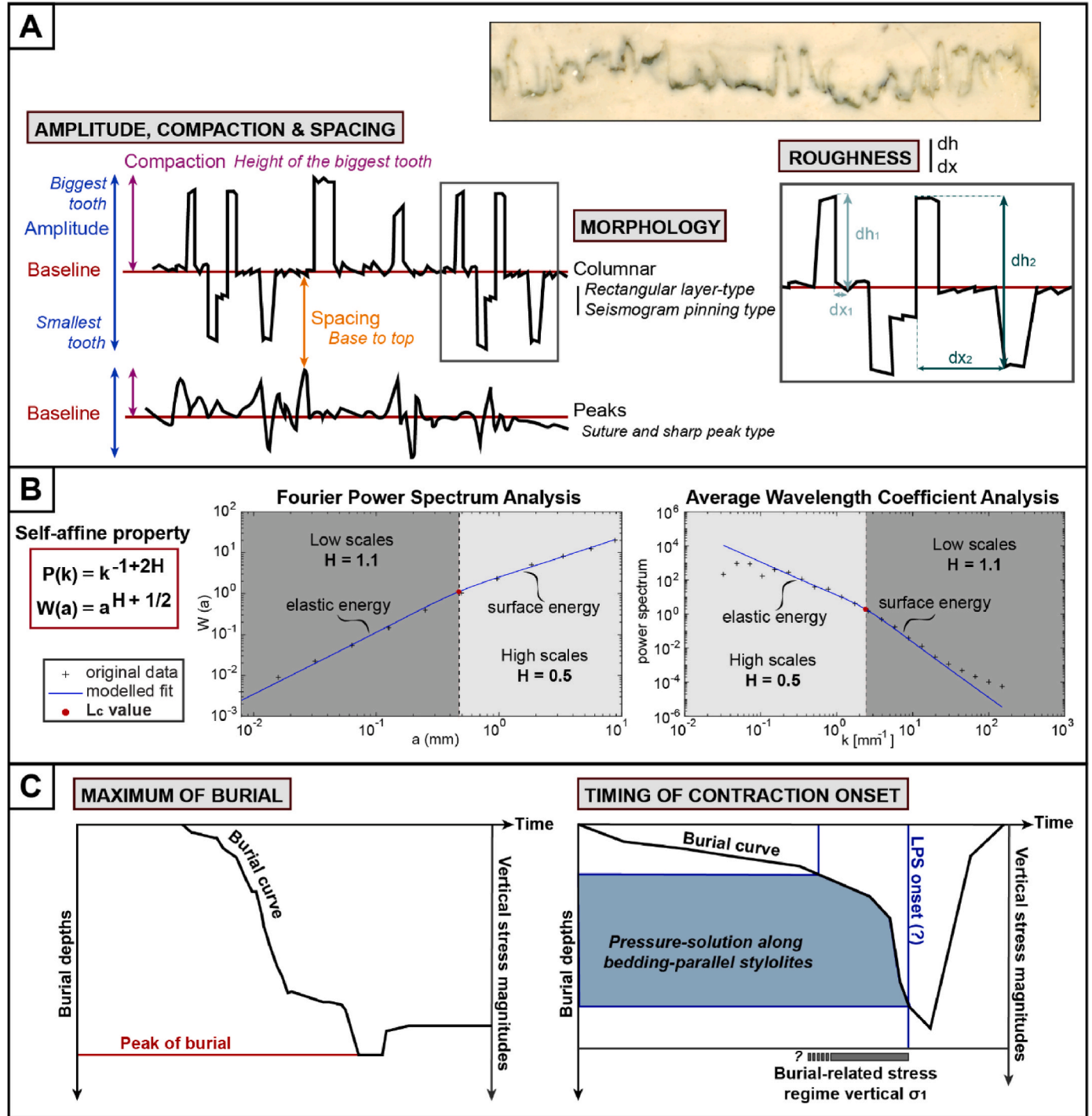


Fig. 1. (A) Photograph of stylolite, illustrating a sketch that defines the physical and morphological characteristics of stylolites, including amplitude, morphology, roughness and spacing. (B) Representation of the two scale regimes on the Fourier Power Spectrum (FPS) and Average Wavelength coefficient (AWC), associated with Hurst coefficients and separated by a characteristic cross-over length. Self-affine property is defined on the left-hand side for each signal analysis. (C) Contributions of SRIT applied on BPS: using burial curves built for each case study, the technique yields either the maximum burial depth recorded by rocks from a poorly deformed intracratonic basin (e.g. the Paris Basin) or helps constrain the timing of tectonic deformation, especially the onset of layer-parallel shortening, in a foreland (e.g. the UMAR).

valid alternative for estimating the paleo burial depth of given strata when compared to methods such as low temperature thermochronology, vitrinite reflectance or organic matter analysis, that derive depth using an estimate of the past geothermal gradient. SRIT becomes more relevant in areas like fold-and-thrust belts, where it is highly challenging to estimate the past geothermal gradient (e.g., Naeser and McCulloh, 2012; Tissot et al., 1987; Yalcin et al., 1997; Beaudoin and Lacombe, 2018) because it is affected by uplift and erosion (e.g., Roure et al., 2010; Beaudoin et al., 2020b).

The defining application case of the Cirque de Navacelle (Ebner et al., 2009b) demonstrated that L_c can reliably be obtained by analyzing the 1D track of a stylolite by the Fourier Power Spectrum (FPS), and by the Average Wavelength Coefficient (AWC) with Daubechies D4 wavelets (Simonsen et al., 1998). These methods enable one to determine the L_c value with 23% of uncertainty (Rolland et al., 2014). Since then, several studies have highlighted significant differences in the L_c values according to the signal analysis methodology used (e.g. Beaudoin et al., 2019), and most of the time favored FPS analysis (e.g. (Beaudoin et al., 2016, 2020b; Bah et al., 2023; Zeboudj et al., 2023), as it was associated to the lowest error relative to the quantification of L_c value (Rolland et al., 2012). In addition, there seems to be a direct influence of stylolite morphology over L_c values resulting from signal analysis (e.g. Beaudoin et al., 2019; Bah et al., 2023). In all cases however, stress results derived from the chosen methodology were found to be consistent with independent geological markers, whether it was related to the depth evolution or to the timing of the onset of tectonic contraction (Beaudoin et al., 2020c).

Considering the important constraints provided by SRIT applied to BPS, especially when coupled to basin-scale burial-time models, we

believe it is timely to provide the structural geology community with a quantitative and critical assessment of SRIT, refining the methodology to facilitate its use in structural studies.

In this work, we applied both the AWC and FPS methods of signal analysis on a large population of BPS ($n = 186$, Table S1) mainly collected in four folded structures ($n = 176$) throughout the Umbria-Marche Apennine Ridge (Apennines, Italy, Fig. 2A), with the addition of a few samples (Corona Anticline, near Perugia and the Gubbio Fault zone, $n = 10$). Pressure-solution was subjected to early classification in the region (Alvarez et al., 1978) which since then has also been the target of a number of paleopiezometric studies conducted using stylolites to reconstruct the depth and timing of early contractional deformation at fold scale, along with the duration of the so-called folding event (encompassing the layer parallel shortening stage, fold growth, and late stage fold tightening; Beaudoin et al., 2016, 2020a; Labeur et al., 2021; Lacombe et al., 2021). We define two criteria that can be used to assess the quality and reliability of the L_c value given by the inversion process for each stylolite: (i) the validity, when the inversions return well defined regression lines of which the slope is consistent with the Hurst exponents; (ii) the consistency, when the results obtained by the FPS and the AWC are consistent with each other's, considering the 23% methodological uncertainty. We then confront the statistically significant highest depths of active pressure solution to local burial-time models to (1) discuss potential reasons for which BPS could have stopped developing, and (2) estimate at what time horizontal tectonic contraction (i.e. Layer-Parallel Shortening) started across the belt. The latter sequence, compared to the well-constrained tectonic calendar of regional folding and thrusting, further supports this combination as a reliable tool to estimate the timing of the early folding contractional

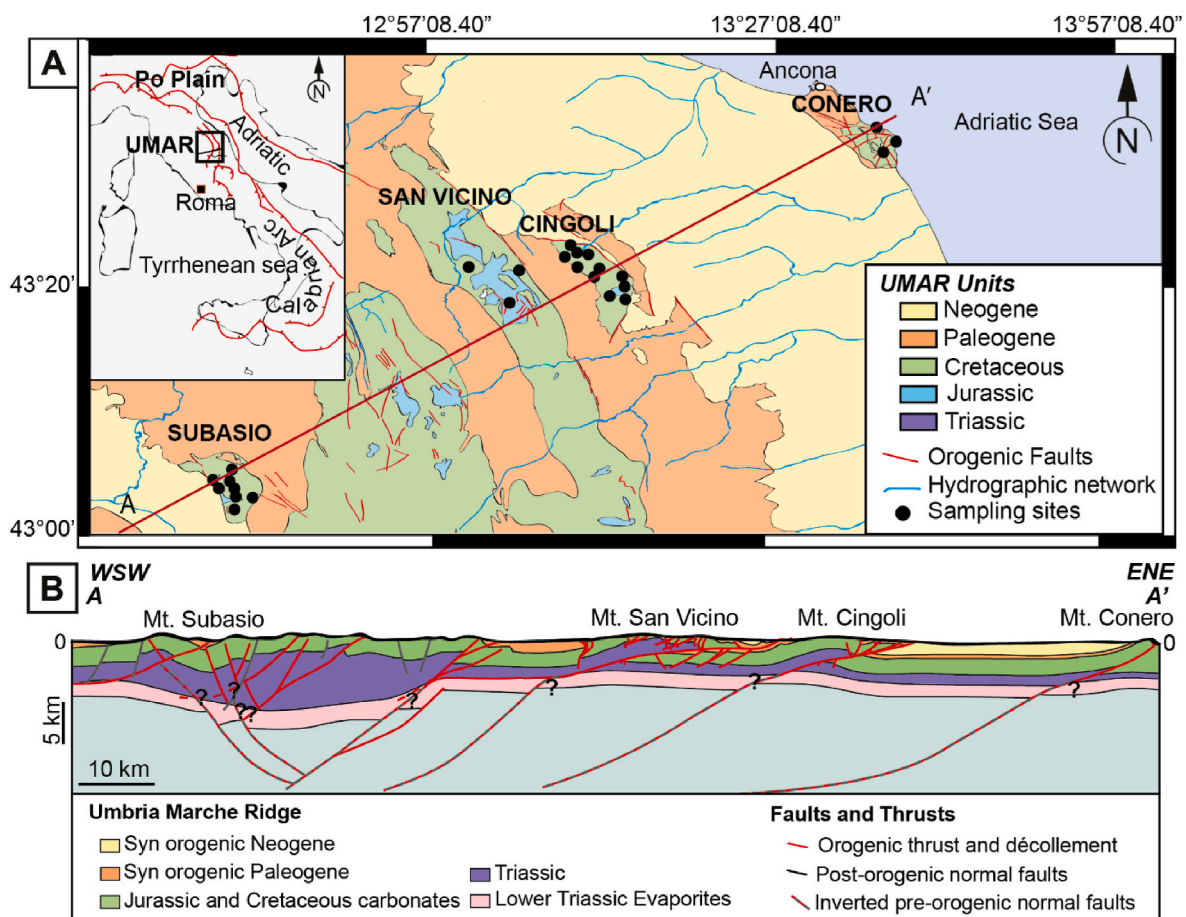


Fig. 2. (A) Simplified geological map of the Umbria-Marche area (after Beaudoin et al., 2020) where are located the sampling sites in the four main structures of this study, along with the cross-section profile. (B) Simplified crustal scale cross section after Scisciani et al. (2014).

deformation and progressive orogenic stress transfer into forelands.

2. Geological setting

2.1. Geodynamic and tectonic setting

Resulting from the convergence of Eurasian and African plates, the Apennines are a mountain belt extending from the Po Plain to the Calabrian Arc over a distance of 1500 km (Lavecchia et al., 1988; Elter et al., 2012). The Apennines are commonly divided in the Northern and the Southern Apennines because of different geological and structural characteristics (Boccaletti et al., 2005; Mazzoli et al., 2006; Satolli et al., 2014). The southernmost area of the Northern Apennines is a succession of paleo-domains that are stacked onto each other by top-to-the-east thrusting, and which are named from west to east as the Ligurian, Tuscan, and Umbria-Marche. The Umbria-Marche Apennine Ridge (UMAR) is a 450 km long fold-and-thrust belt with eastward convexity and displaying a succession of east-verging anticlines separated by narrower synclines (Scisciani et al., 2014) (Fig. 2A). Its outermost active contractional part is located offshore in the Adriatic Sea, while post-orogenic extension currently affects its innermost part (Lavecchia et al., 1988; Cello et al., 1997; Ghisetti and Vezzani, 2002; Tavani et al., 2012, Pace et al., 2017, 2022; Sabbatino et al., 2021). The Late Oligocene to Pleistocene onshore shortening across the UMAR (Lavecchia et al., 1988; Brozzetti et al., 2021) has been estimated on the basis of restored cross sections to up to 10% (Scisciani et al., 2014), yet the structural style of deformation for the UMAR, either thin-skinned or thick-skinned, has long been debated (e.g. Tozer et al., 2002; Scisciani

et al., 2006; Lacombe and Bellahsen, 2016, Fig. 2B) until recent studies supported that both styles were involved during the building of the chain (Barchi and Tavarnelli, 2022). The assumption of thrusts rooted on inherited pre-orogenic structures, mostly pre-existing normal faults formed either during the evolution of the Mesozoic passive margin or during the foreland flexure, is also suggested in several studies (Hippolyte et al., 1995; Tavarnelli, 1996a; Tavarnelli, 1996b; Mazzoli et al., 2000; Scisciani et al., 2001; Calamita et al., 2003; Rusciadelli et al., 2005; Pace and Calamita, 2014).

2.2. Sedimentary and structural setting

The characteristic succession of the UMAR, a carbonate-dominated succession deposited from the earliest Jurassic to Oligocene (Fig. 3A) (Lavecchia et al., 1988; Santantonio, 1993; Carminati et al., 2010), consists of four main sedimentary units: (i) the pre-rift Triassic-Mid-Jurassic sequence, that includes evaporites considered as the main décollement level. Up to 5 km of evaporites can be found in the central part of the UMAR (Scisciani et al., 2014, Fig. 2B); (ii) the syn-rift Mid Jurassic-Cretaceous pelagic sequence, (iii) the post-rift Upper Cretaceous-Paleogene pelagic sequence; and (iv) the Miocene hemipelagite and turbidite deposits which recorded the progressive eastward involvement of the Meso-Cenozoic succession into the fold-and-thrust belt and its associated foreland basin to the East (Calamita et al., 1994; Bigi et al., 2009). A thickness of more than 3000 m of turbidite deposits ahead of the advancing fold-and-thrust belt during foreland flexure (Sabbatino et al., 2021). The studied strata belong to the Umbria-Marche succession (Fig. 2B). In stratigraphic order, this

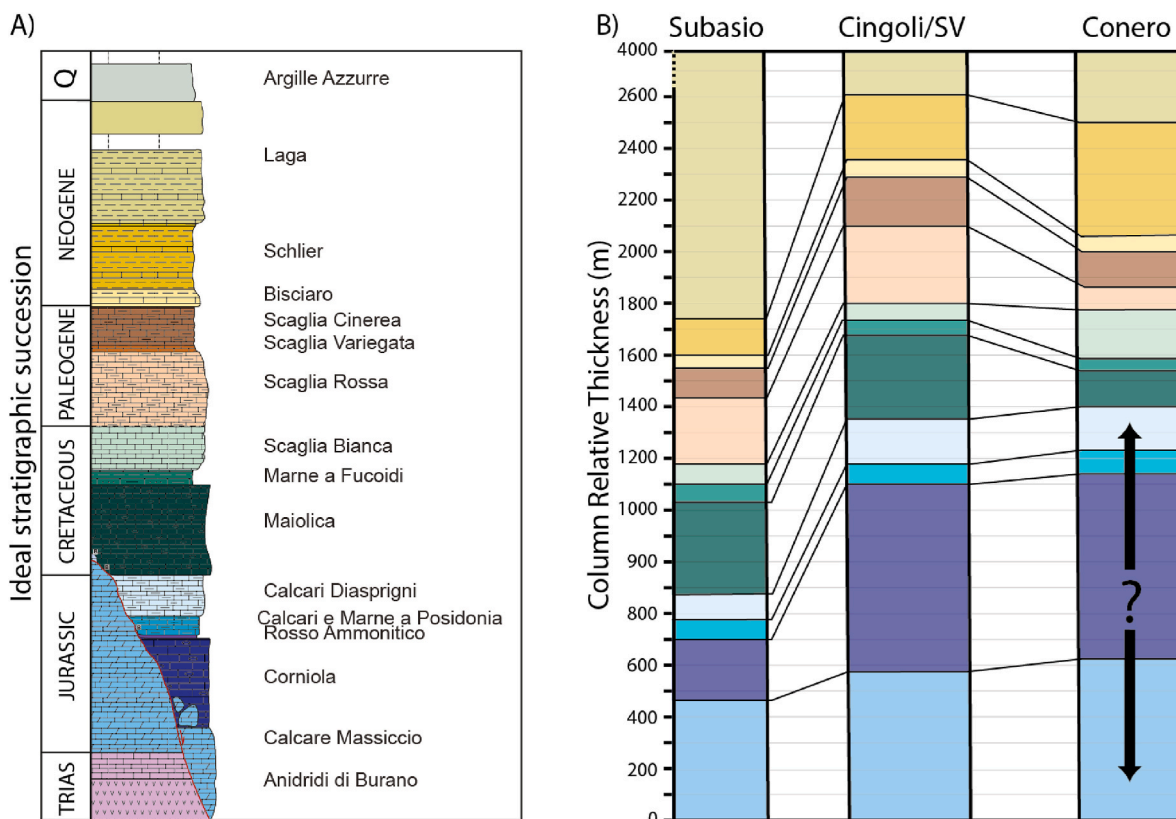


Fig. 3. (A) Ideal stratigraphic column, not to scale, showing the whole Umbria Marche sedimentary succession (in the area of Cingoli Anticline, after Labeur et al. (2021) modified from Petracchini et al. (2012)). (B) Relative overburden of the stratigraphic succession considering the Massiccio Formation as the 0 (bottom) and the Laga Formation as the top. This represents the current stratigraphic thickness of each unit of interest (Jurassic – Paleogene) for the area of the Subasio Anticline (after the geological map, sheet 123 from the Servizio Geologica d'Italia, 1969), the Cingoli/San Vicino pair (after Petracchini et al., 2002) and for the Conero Anticline (after Fancelli and Radrizzani, 1964a, b).

succession comprises the pre-rift Calcare Massiccio, 700 m-thick massive limestone deposited in peritidal environments. Sealing the rifting that affected the Calcare Massiccio, a few formations compose the Umbria-Marche pelagic succession. (i) The Sinemurian-Pliensbachian biomicritic limestones with chert bed intercalations of the Corniola Fm.; (ii) the Toarcian Rosso Ammonitico Fm., composed by nodular marly limestones; (iii) Aalenian marls and cherty limestones of the Calcari e Marne a Posidonia Fm.; (iv) Bajocian to Oxfordian Calcari Diasprigni Fm., radiolarian-rich cherty limestones evolving from towards micritic limestones and marls, and (v) Tithonian Calcari a Saccoma e Aptici Fm. Note that the Hettangian to Tithonian succession is condensed on the platform and referred to as the Bugarone group (Lavecchia et al., 1988; Alvarez, 1989; Cipriani et al., 2019). During the early Cretaceous, micritic limestones of the Maiolica Fm., and marls of the Marne a Fucoidi Fm., were successively deposited. The overlying Cretaceous to Paleogene Scaglia Group is subdivided into four successive members which end the Umbria-Marche succession: (i) the Scaglia Bianca; (ii) the Scaglia Rossa; (iii) the Scaglia Cinerea and (iv) the Scaglia Variegata (Alvarez et al., 1977). Above these pelagic deposits, the flysch, namely, the Bisciaro, Schlier and Marnoso-Aranacea formations, deposited during the Pliocene contraction in an asynchronous fashion with an eastward younging (Guerrera et al., 2012). Deposition started in the late Burdigalian in the belt, and in the Serravallian on the Adriatic coastline. For more detailed information about the sedimentary history of the UMAR, please refer to e.g. Conti et al. (2021).

The establishment of the timing and sequence of deformation in the UMAR has been initially done by the structural investigation of thrusts and folds and dating of the related growth strata (Calamita et al., 1994; Mazzoli et al., 2002). Further insights came from the analysis of the mesoscale fracture-stylolite network that established a relative sequence within each fold (Decandia et al., 2002; Tavani et al., 2008; Díaz General et al., 2015; Beaudoin et al., 2016; Labeur et al., 2021; Lacombe et al., 2021) and across the ridge (Beaudoin et al., 2020a) that were further constrained by the use of U–Pb geochronology applied on synkinematic calcite in veins and faults (Beaudoin et al., 2020a; Labeur et al., 2021; Lacombe et al., 2021). The following five stages of deformation were recognized: (i) the foreland flexure stage, dated from late Oligocene-early Miocene in the western part of the ridge (i.e., eastern Tuscany-Monte Subasio) and from the middle Miocene in the eastern part of the ridge (i.e., Gubbio, Monte Nero, San Vicino, and Cingoli areas (Tavani et al., 2015; Brozzetti et al., 2021)). Some early mesostructures including joints, veins, and dilation deformation bands perpendicular to bedding, as well as mesoscale faults, can be related to this extensional stage (Tavani et al., 2015); (ii) the early-folding layer-parallel shortening (LPS) stage, under a NE-SW-oriented Apenninic contraction (Marshak et al., 1982; Tavarnelli, 1997; Storti et al., 2001; Tavani et al., 2008; Barchi et al., 2012), occurred from the Burdigalian to the West, and from the Tortonian to the East (Brozzetti et al., 2021). Fractures related to LPS include vertical veins oriented perpendicular to bedding, while postdating BPS; they are striking NE-SW (i.e. perpendicular to the strike of the fold axis) and are associated with bed-perpendicular tectonic stylolites with peaks trending NE-SW and plunging parallel to bedding dip (Beaudoin et al., 2020a; Labeur et al., 2021). These veins were dated by U–Pb calcite geochronology at 6.1 ± 2 Ma in the San Vicino Anticline (Lacombe et al., 2021); (iii) the folding stage, starting at the Langhian time in the western part and at the Messinian time in the eastern part of the UMAR. This stage is characterized by a maximum compressional stress oriented NE-SW (Tavani et al., 2012), i.e. parallel to regional shortening, and local extension perpendicular to fold axes associated with strata curvature at fold hinges (Beaudoin et al., 2020a). NW-SW-striking veins, bed-perpendicular and parallel to the fold axis, were linked with folding, and dated at 3.5 ± 1 Ma in San Vicino (Lacombe et al., 2021); (iv) the Late Stage Fold Tightening (LSFT), still associated with a NE-SW contractional trend, corresponding to the moment when shortening is no longer accommodated, by e.g. limb rotation (Tavani et al., 2015; Beaudoin et al., 2020a). Vertical, NE-SW

striking veins, kinematically consistent with tectonic stylolites with a vertical plane and peaks trending NE-SW, were dated at 3.7 ± 0.3 Ma in the San Vicino (Lacombe et al., 2021). Also strike-slip faults that developed during the LSFT were dated $\sim 5 \pm 1$ Ma in the Camerino syncline, located just at the rear of the San Vicino anticline (Beaudoin et al., 2020b); (v) the post-orogenic extension, starting by Pliocene times in the western UMAR (Barchi et al., 2012) and continuing westward today. This extensional stage is associated with NNW-SSE striking normal faults causing the downfaulting of the fold succession (Bally et al., 1986; Calamita and Deiana, 1988; Barchi et al., 2012).

3. Sample collection and preparation

A dataset comprising a total of 186 BPS distributed along a SW-NE cross section across the central portion of the UMAR is used for this study, including some previously published data (Labeur et al., 2021; Beaudoin et al., 2020b (Fig. 2A–Table S1)). Mainly, four folded structures were sampled (Fig. 2). From West to East, Monte Subasio (39 BPS in the Maiolica and Scaglia Fms.), Monte San Vicino (28 BPS in the Maiolica Fm.), Monte Cingoli (77 BPS in the Maiolica and Scaglia Fms.), and Monte Conero (32 BPS in the Maiolica and Scaglia Fms). In this dataset, only 7 BPS come from Monte Subasio, and the ones from Monte Cingoli were published before, hence 102 new stylolites are introduced in the dataset considered in this study.

The sampled carbonates show mud-supported textures (mudstone to wackstone) in which early mesoscale deformation is mainly accommodated by pressure-solution (Fig. 3). Stylolites of various morphologies (following the classification of Koehn et al., 2016), i.e. seismogram pinning type (2) or suture and sharp peak (3) types (Fig. 1), and origin (tectonic or sedimentary) were recognized (Fig. 3). The chronological relationships established in the field show that the studied BPS predate bed-perpendicular veins oriented perpendicular to the fold axis, that likely developed during the LPS (e.g. Decandia et al., 2002; Tavani et al., 2006; Beaudoin et al., 2020a). Type 2 and type 3 morphologies were not restricted to specific sampling sites. Sampling was carried out on blocs using a hammer and chisel to preserve the stylolite morphology from damages induced by vibrations of a portable core-drill. For each sampling site, the orientation of the bedding S_0 was measured as well as the strata polarity. Selected hand samples comprise isolated BPS tracks, with peaks locally striking perpendicular to their plane, so with negligible shearing during or after pressure-solution (Koehn et al., 2007). The samples displaying dominantly anastomosed stylolites or stylolites cut by veins were discarded for the SRIT.

In order to apply SRIT, samples were prepared in two steps: (1) samples were cut perpendicular to the stylolite plane. A single cut is required to perform the inversion in the case of BPS; however 2 perpendicular cuts were made on randomly selected samples to check the similarity of L_c values in both planes and so the in-plane stress isotropy, a prerequisite to apply the SRIT to BPS (Ebner et al., 2009a); (2) the cut faces were polished and the stylolite tracks scanned at high resolution (12,800 dpi).

4. Methods

4.1. Petrography and diagenesis

The petrography and the diagenetic state of the collected carbonate samples were checked on 69 thin sections (30 μ m thickness) cut on the mirror face of the scanned surface. Classical optical microscopy was performed on a Nikon BH2 microscope equipped with a Nikon MK1 camera, and cathodoluminescence was performed with a cold cathode Cathodyne CITL CCL 8200 Mk4 coupled with a Sony Alpha III camera. Observations were carried out at the LFCR (Université de Pau et des Pays de l'Adour, France).

4.2. Stylolite roughness inversion technique

The studied population of 186 BPS is characterized by stylolites displaying mainly a suture and sharp peak morphology (75%, versus 25% seismogram pinning). The application of SRIT to stylolite roughness for stress requires the reliable estimate of the cross-over length L_c (Schmittbuhl et al., 2004). The process starts with the digitization of the stylolite track by means of an image-analysis routine that uses color thresholding tools to isolate the stylolite from the surrounding host rock. In case this process fails, the stylolite track is hand-drawn following the protocol presented in Ebner et al. (2009b).

The stylolite track is then transformed into a distance-height matrix that represents the top part of the stylolite track. To facilitate signal processing, the baseline of the track is corrected from the average trend of the track (e.g. Ebner et al., 2009a; b; Rolland et al., 2012) by applying the difference between the local height of the track and the best straight-fit line. This process is repeated until the average trend of the track is as close as possible to the horizontal. Finally, the whole average trend is set to a vertical value of 0. The corrected track is then processed by either Fourier Power Spectrum or Average Wavelet Coefficient methods. The FPS considers the track as a sum of periodic sines and cosines from which a wave number k (mm^{-1}) and the squared Fourier transform modulus $P(k)$ are extracted. The AWC technique uses the Daubechies D4 wavelet to consider the signal as a sum of different wavelets originating from a mother function (Simonsen et al., 1998), from which the scale a (mm) and the average wavelet coefficient $W(a)$ are extracted. Log-log plots $P(k) = f(k)$ and $W(a) = f(a)$ are used to bin the raw data at a given interval (1.5 after Ebner, 2009). As both signal processing methods can be used to estimate the Hurst coefficient (i.e. the slope of the binned data) using the relationships given in Fig. 1B valid in log-log space ($P(k) = k^{-1-2H}$ and $W(a) = a^{0.5+H}$), we used a non-linear least-square regression with fixed value of H to estimate the value of L_c , i.e. the scale at which one slope changes to the other slope.

The crossover length value estimated in mm by the signal processing approach (Renard et al., 2004; Schmittbuhl et al., 2004; Ebner et al., 2009a, 2009b) is directly related to the magnitude of the prevalent mean stress σ_m and differential stress σ_d in the strata at the time the stylolite stopped to be an active dissolution surface (Equation (1)):

$$L_c = \frac{\gamma E}{\beta \sigma_m \sigma_d} \quad (\text{equation 1})$$

where L_c is the crossover length (in mm), E the Young modulus of the rock (in Pa), γ is the solid-fluid interfacial energy (in $\text{J}\cdot\text{m}^{-2}$), β a dimensionless constant depending on the Poisson ratio (ν) ($\beta = \frac{\nu(1-2\nu)}{\pi}$), σ_m the mean stress magnitude ($\sigma_m = \frac{\sigma_1 + \sigma_2 + \sigma_3}{3}$) and σ_d the differential stress magnitude between σ_1 and either σ_2 or σ_3 according to the orientation of the studied track.

Assuming a vertical attitude of the maximum principal stress σ_1 related to burial at the time of BPS development, the calculation of σ_1 magnitude is based on the uniaxial strain hypothesis which implies no horizontal strain within the plane of the stylolite so that the horizontal stresses σ_H and σ_h are equal in the plane of the stylolite ($\sigma_h = \sigma_H = \frac{\nu}{1-\nu} \sigma_1$). This hypothesis is valid at first order as BPS are supposed to form during the basin formation in response to burial only. However as tectonic stress may apply at the boundaries of the basin, we need to check the validity of this hypothesis by studying two tracks cut at an angle on the same stylolite, that should return the same L_c value if the in-plane stress is isotropic (i.e. $\sigma_2 = \sigma_3$; e.g. Beaudoin et al., 2016). Under this assumption, the differential stress σ_d is always the same regardless of the orientation of the studied track, and Equation (1) can be simplified as follows:

$$\sigma_v^2 = \frac{\gamma E}{\alpha L_c} \quad (\text{equation 2})$$

with α defined as $\alpha = \frac{(1-2\nu)(1+\nu)^2}{30\pi(1-\nu)^2}$.

Equation (2) therefore yields the value of the vertical stress, i.e. the lithostatic stress, applied to the rock at the end of stylolite development, that can be converted into the overburden value (z) using $z = \frac{\sigma_v}{\rho g}$ (equation 3).

Considering equation (2) and the uncertainty of 23% quantified for the L_c value (Rolland et al., 2014), the propagation of the uncertainty allows to fix the uncertainty associated with σ_v estimate at 12% if assuming no uncertainty on E , ν , or γ .

4.3. Rock mechanical properties

In order to solve equation (2), the Young modulus (E) must be estimated, as it is the most uncertain elastic parameter considering carbonate rocks (Regnet et al., 2019). To do so, we use the non-destructive Schmidt hammer, that measures the rebound of a spring-loaded piston when pressed orthogonally against the surface of a rock. The rebound value R is considered to be a proxy of the surface stiffness and consequently allows the calculation of E following an empirical relationship (e.g. Sachpazis, 1990; Katz et al., 2000; Aydin and Basu, 2005). In this work, we have used the equation of Katz et al. (2000):

$$E = 0.00013 \times R^{3.090704} \quad (\text{equation 4})$$

A Silver Schmidt OS8200 type N (manufactured by PROCEEQ) was used on 11 sites in Jurassic and Cretaceous formations in the Subasio and Conero anticlines, in order to complement the previously published dataset for San Vicino and Cingoli anticlines (Labeur et al., 2021). In each site, 40 to 50 rebounds were performed perpendicularly to the surface, in most cases flat-lying (i.e., the hammer being vertical), from which rebound values were averaged as a single rebound value valid for the site. In order to ensure that this value is free from any outlier due to local heterogeneity, we calculated a moving average incremental mean until the mean rebound value stabilizes.

4.4. Burial-time models

To reconstruct the burial evolution of the sampled formations (Maiolica, Corniola and Scaglia fm.) over time, we have built 1-D burial-time models for all four folded structures using the TemisFlow basin modeling software. The burial-time simulation follows two steps: first, a backward modeling, consisting of the backstripping the stratigraphic column that includes a progressive decompaction of the sediment (or compaction in case of erosion) as the overlying strata are removed from the youngest to the oldest. Decompaction is calculated following porosity vs depth or compaction curves (Atashbari and Tingay, 2012), that predicts the thickness of a strata according to its lithology, with respect to physical and chemical processes that affect compaction. This backward modeling is done under the assumption that a hydrostatic pressure regime prevails at the basin scale (Perrier and Quiblier, 1974). The second step consists of a forward simulation of the sequence of deposits and associated erosion considering the geodynamic history that affected the sedimentary stack, in other words, it is a simulation of the burial evolution of each formation of interest.

At each folded structure (Subasio, San Vicino-Cingoli and Conero), and for every formation since the Jurassic (Massiccio Fm), thickness and related age of deposition have been defined from the published stratigraphic sections (Fig. 3) considering the most preserved stack (i.e. not in the fold-hinge). Exception was made for the Conero Anticline, where the oldest considered formation is Cretaceous in age (Maiolica fm). The rock properties (initial porosity, solid density) and the constitutive law of each formation's average lithologies are reported in Table S2. We selected an average compaction law adapted for limestones based on an empirical model that accounts for both mechanical and chemical compactions, issued from compilation of carbonates porosity measurements at different depths (e.g. Atashbari and Tingay, 2012). The erosional

events, the most uncertain parameters in terms of removed thickness on the folded structures, were defined from literature (Mazzoli et al., 2002; Brozzetti et al., 2021).

5. Results

5.1. Petrography

In all studied folds, microscopic observations under classical microscope reveal mud-supported carbonates in both Miaolica, Scaglia Bianca and Scaglia Rossa fms. (Fig. 4). Mudstone to wackestone texture are documented, with numerous foraminiferae in the Scaglia formation, blocky calcite veins, and sedimentary or tectonic stylolites surrounded by an altered area (Fig. 4). These are ideal texture for the use of SRIT as suggested in Beaudoin et al. (2019) and Bah et al. (2023). Under cathodoluminescence, both host rocks and veins are dull orange, with neither evidence of recrystallization events nor alteration related to diagenesis like dissolution or mineralogical replacement.

5.2. Young modulus estimates

In 15 sites in the Subasio and Conero anticlines, 542 R rebound values were measured on flat homogeneous surfaces to estimate rock elastic properties for the Maiolica, Scaglia Bianca, Scaglia Rossa formations. These representative R values and the resulting calculated Young moduli are reported in Table S3. R values range at Subasio from 54 to 59 in the Maiolica Fm., and from 49 to 65 in the Scaglia Rossa and

Bianca Fms. At Conero, R values for the Maiolica Fm. Range from 53 to 62. In the Cingoli anticlines, R values for the Maiolica Fm. Range from 36 to 52, and from 50 to 70 in Scaglia Rossa and Variegata Fms (from Labeur et al., 2021), and are estimated to be similar in the nearby San Vicino anticline. The curves associated with the values from Subasio and Conero are available as supplementary material (Fig. S1).

Using these values with equation (4) returns an overall range of E values from 14 GPa to 17 GPa in Cingoli Anticline (average $E = 15$ GPa), from 18 to 45 GPa in Subasio Anticline (average $E = 29$ GPa), and from 23 to 37 GPa in Conero Anticline (average $E = 30$ GPa). These average values are 10–25% higher than the 23 GPa value found by Beaudoin et al. (2016) by applying SRIT and VP/Vs inversion in the Monte Nero Anticline, located in the western part of Central UMAR, suggesting a rather homogeneous distribution of the elastic properties of the UMAR succession despite the intrinsic natural variability of carbonates.

5.3. Cross-over length estimates

186 stylolites of which the width distributes between 0.6 and 12 cm, with a modulus value of 3 cm, were used for the SRIT using both signal processing methods, i.e. FPS and AWC (Table S4). Two values of L_c were therefore obtained for each BPS analyzed.

Out of the 186 tracks analyzed with both FPS and AWC, 167 are valid, i.e. both self-affine regimes are fitted through the binned data (Fig. 5). 85% of the inversions are thus conclusive. Among the 29 invalid treatments, 7 are for AWC only (i.e. 4% of the 186 initial data), 13 for FPS only (i.e. 7%), and 9 for both (i.e. 5%) (Fig. S2).

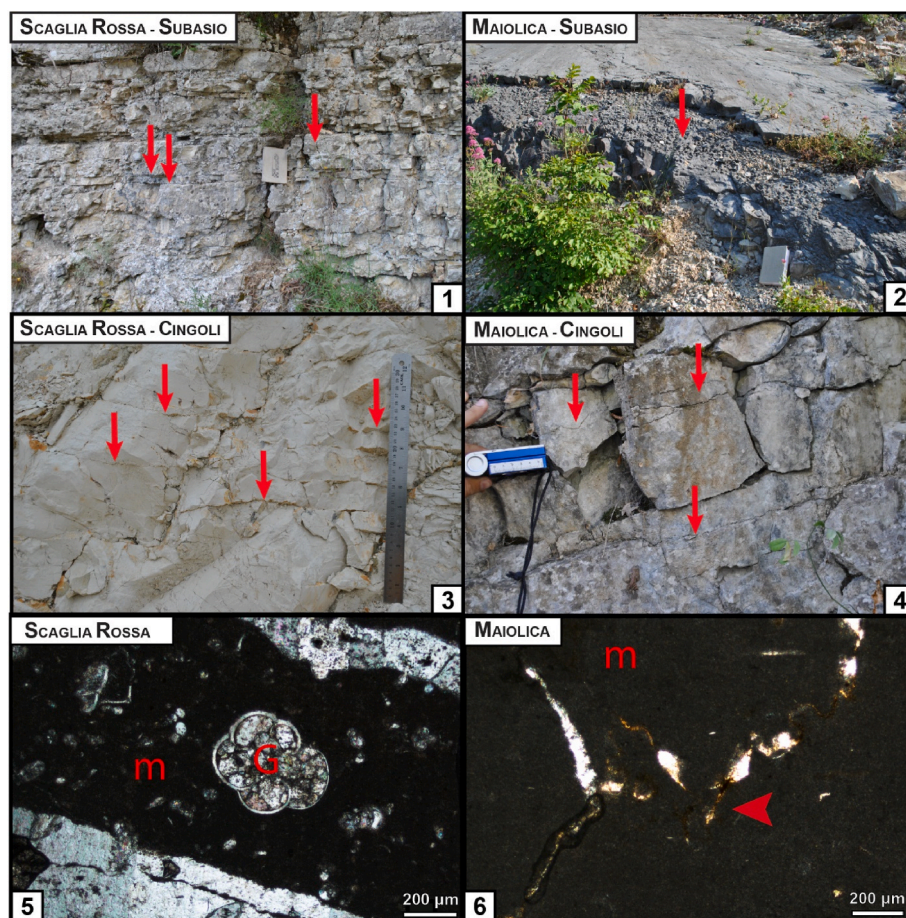


Fig. 4. (1–4) Field photographs of the Maiolica and Scaglia Rossa formations as observed in both Subasio and Cingoli anticlines, with the red arrows pointing at bedding parallel stylolites. (5–6) microphotographs (in natural polarized light) of the Maiolica and the Scaglia Rossa formations that show a mudstone-wackestone texture with a micritic matrix (m) and the occurrence of Globigerina (g). The red arrow points at a bedding parallel stylolite. (For interpretation of the references to color in this figure legend, the reader is referred to the Web version of this article.)

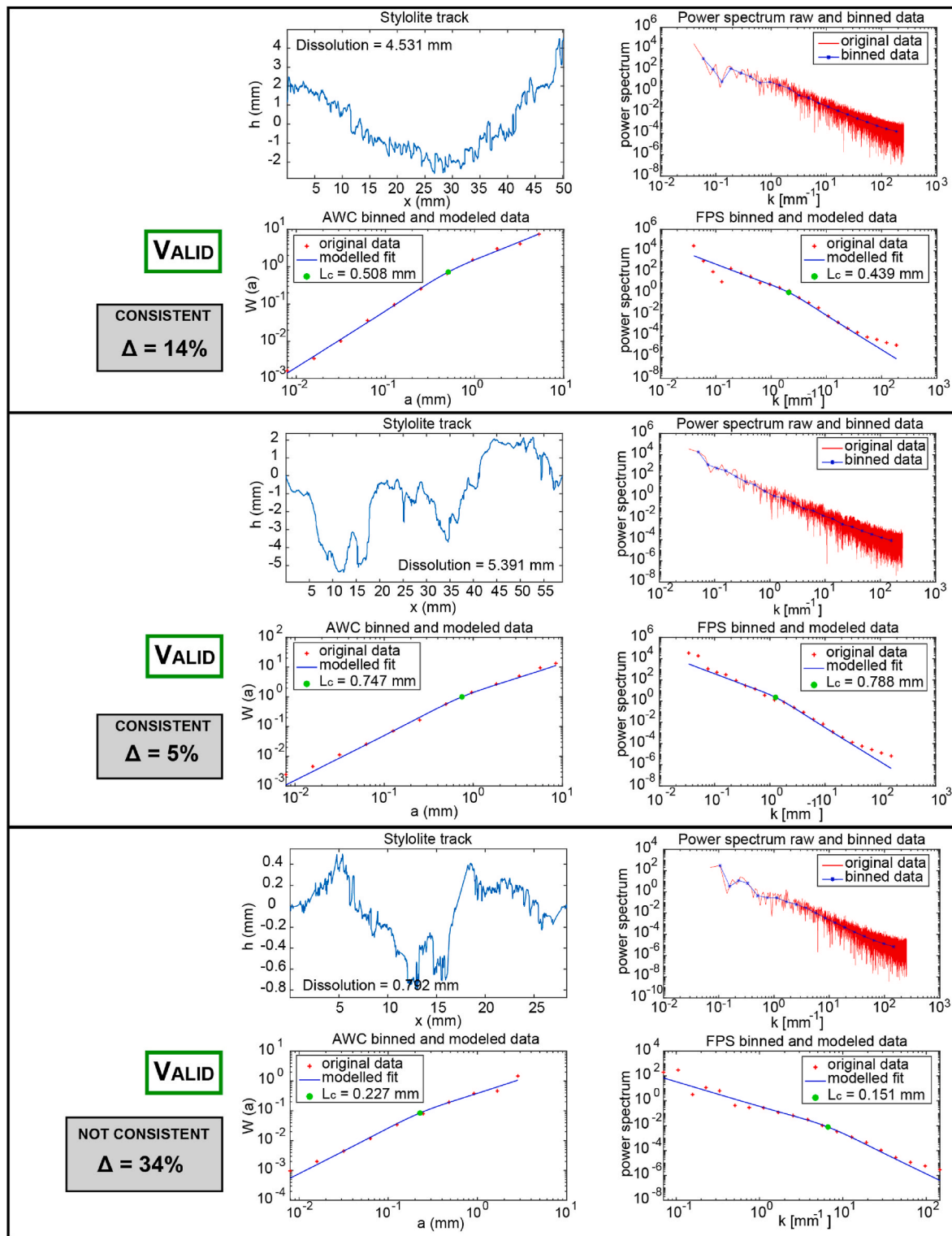


Fig. 5. Selected examples of application of stylolite roughness inversion techniques that returned a valid inversion result (i.e.; two lines with set slopes). For each example, are reported from top left to bottom right: the track of the stylolite with an estimate of the minimum dissolution; the signal analysis with Fourier Power Spectrum with original and binned data following the protocol established by Ebner (2009); the plot of the binned data using the Average Wavelet Coefficient signal analysis, with in blue the modelled regression line that is constrained by 2 preset roughness coefficients (Hurst exponents), returning the L_c value (green star); plot of the FPS binned data with in blue the modelled regression line that is constrained by 2 preset roughness coefficients (Hurst exponents), returning the L_c value (green star). For each example, the Δ value is reported (see text for details), and defines if the inversion is consistent ($\Delta < 23\%$) or not consistent ($\Delta > 23\%$). (For interpretation of the references to color in this figure legend, the reader is referred to the Web version of this article.)

The variations of L_c values were also considered against the morphology of the stylolites analyzed. The morphologies considered are “seismogram pinning type” and “suture and sharp peak type”, corresponding to type 2 and 3 in the classification of Koehn et al. (2016), respectively. Both types of morphologies were observed in all the sampling sites.

The use of violin plot, of which the envelope represents a probabilistic modeling of the population based on its limited statistical distribution, allows to determine if the population is likely to follow a unimodal or bimodal distribution model (Hintze and Nelson, 1998). Fig. 6A shows differences in L_c values according to the stylolite morphology: for seismogram pinning type (type 2) the distribution is bimodal (violin plot envelope shows two separated bumps) and L_c values are higher (considering median and quartile values), for suture and sharp peak type (type 3), the distribution is unimodal (violin plot

envelope show one bump), and the L_c values are lower.

5.4. Burial depth estimates

The crossover lengths L_c values and the corresponding values of the vertical stress were determined using SRIT considering the following mechanical and/or chemical parameters: Young modulus E , estimated from the Schmidt Hammer measurements, averaged for a given formation at the scale of a studied structure (Table S3), Poisson ratio ν and solid-fluid interfacial energy γ fixed to classical values of 0.25 and 0.32 J/m^{-2} (Wright et al., 2001), respectively. Then, the vertical stress values were converted into burial depths following Equation 3. They are rounded to the closest 10 m. Detailed values of vertical stress and burial depth magnitudes are summarized in Table S4. In order to discuss the impact of the variability of E onto the calculated vertical stress

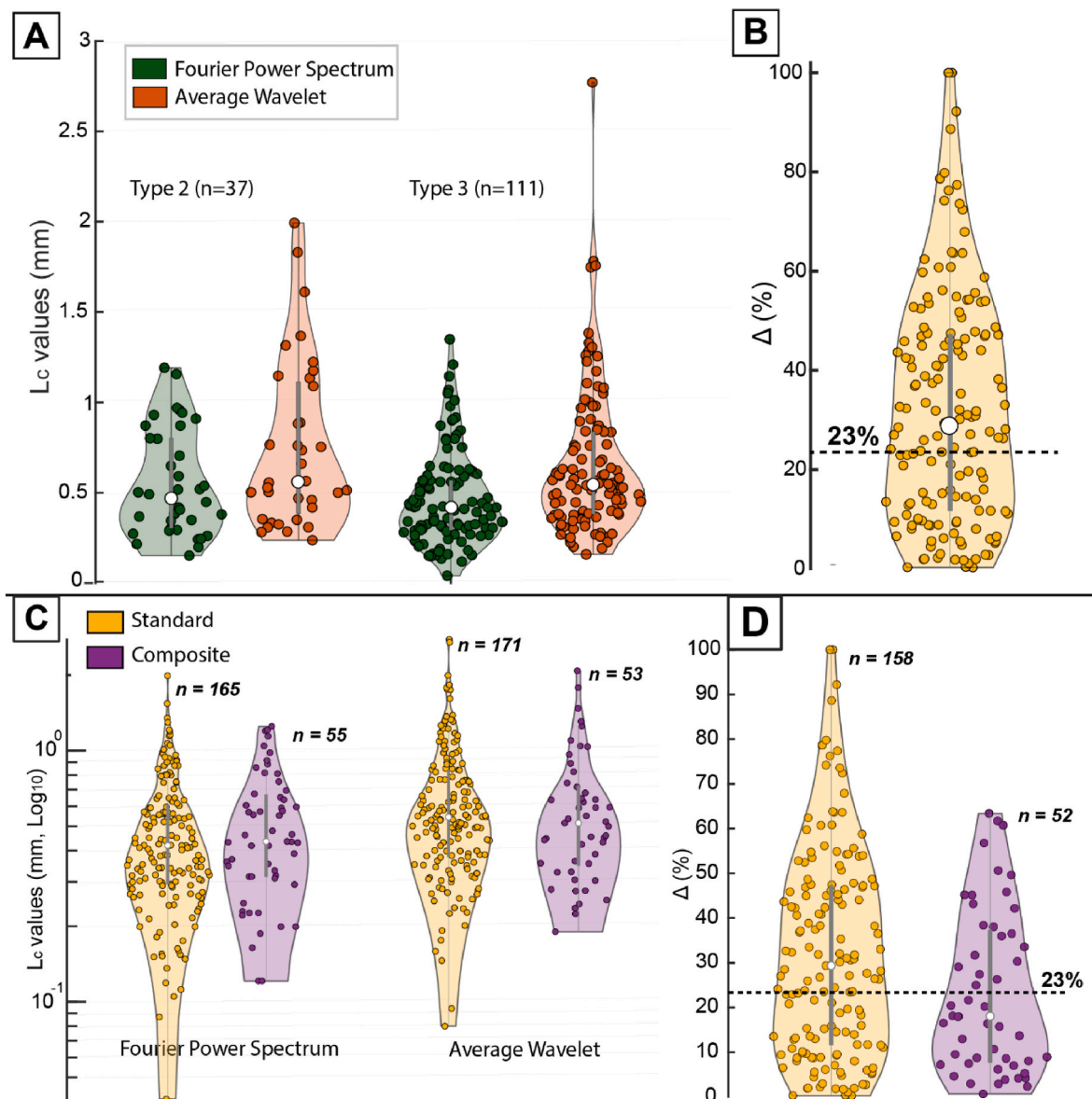


Fig. 6. Violin plots (model of the probabilistic distribution of a population based on a limited population) with whisker and box plots (grey box, white dot is the value of the average for the population) of the whole dataset of BPS. (A) Distribution of the valid L_c values according to the morphology of the stylolite (type 2 or type 3) and to the signal analysis method used. (B) Corresponding distribution of the Δ value, where the consistency criterion is met if a data is below the 23% line reported (see text for details). (C) Distribution of all the L_c values including the not valid ones as a function of if the SRIT was applied to a single track (yellow population) or on a composite track, made by a succession of stylolite of the same morphology found in the same sample (purple), according to the signal analysis methodology. (D) Corresponding distributions of the Δ values according to if the SRIT was applied to a single track (yellow population) or on a composite track (purple population). (For interpretation of the references to color in this figure legend, the reader is referred to the Web version of this article.)

magnitudes, we also considered a value of E fixed to 23 GPa for the whole samples (Beaudoin et al., 2016), of which values are reported in Table S4, with distributions plotted as Supplementary Fig. S2.

Considering local E values, the ranges of maximum depth of stylolite activity are graphically represented in Fig. 7 using violin plots for each formation and locality. In each anticline except in the Conero Anticline, the median burial depths recorded in the different formations are in the same range of values. They vary along the regional transect, with deeper values obtained in Subasio and Conero anticlines and shallower values obtained in San Vicino and Cingoli anticlines.

5.5. Burial-time models

The four burial-time models built (Subasio, San Vicino, Cingoli, and Conero anticlines) are considered representative of the innermost (Subasio), central (San Vicino-Cingoli) and outermost (Conero) parts of the UMAR, respectively (Fig. 8, Table S3). In the innermost area, one can observe first a fast burial rate (112 m/My) concomitant to the beginning of the rifting phase, followed by a gentle burial rate (<30 m/My) that started at the Sinemurian time until 25 Ma ago when a strong subsidence phase begun, with a burial rate of ca. 50 m/My and accelerated to reach a rate of 190 m/My during the Serravalian-Tortonian interval. The maximum depth experienced by the bottom of the Maiolica Fm. is ca. 3700 m. If one considers that the exhumation started with, and is mainly caused by, folding and associated erosion, growth strata indicate that exhumation started at around 7 Ma. In the center-east of the UMAR, the models constructed for the San Vicino and Cingoli anticlines reveal a similar evolution, with the increase of burial rate due to rifting, followed by a slow burial phase that lasted until 20 Ma ago, followed by a phase of high burial rate up to 70 m/My during the building of the UMAR. The maximum burial depth experienced by the bottom of the Maiolica Fm. is ca. 2300 m and the exhumation started ca. 5 Ma ago (Mazzoli et al., 2002; Lacombe et al., 2021). Finally, in the outermost part of the UMAR, the maximum depth reached by the bottom of the Maiolica Fm. is ca. 2500 m. In this area where the thickness of the syn-rift Massiccio Fm. is

not documented, the model reconstructed a mainly slow mean burial rate of 5 m/My until 20 Ma ago when the burial rate jumped up to 150 m/My then to 1300 m/My until 4 My ago. Syn-folding exhumation started 4 Ma ago (Calamita et al., 1994).

6. Interpretation of results and discussion

6.1. Reliability of SRIT applied to BPS

In order to help the community critically interpret the results of SRIT and apply it confidentially, we propose to assess first the reliability of the inversion of the roughness of individual stylolites using the two following criteria.

First, the *validity* of a stylolite roughness inversion is related to the occurrence of a clear breakout in the regression on the signal analysis log-log plot with the Hurst exponents of the two power laws fitting the model proposed by Schmittbuhl et al. (2004, e.g. Fig. 5). Because of data binning and because of the actual signal itself, it might happen that either the signal exhibits only one power law (e.g. Karcz and Scholz, 2003), or there are 2 power laws but with Hurst exponents that do not fit the model, or both. If any of this occurs, then the stylolite roughness inversion is not valid, and L_c must be discarded for the dataset. In the population of 186 stylolites presented in this study, 85% of the dataset, i. e. 157 stylolites, return a valid inversion either using FPS, AWC, or both methods.

Second, the *consistency* of a stylolite roughness inversion is related to the similarity of the L_c values provided by the two signal analysis techniques within the methodological uncertainty of 23% (Rolland et al., 2014). A parameter Δ can be calculated as the norm of the difference between L_c values obtained by different signal analysis methods divided by the highest L_c value, reported as a percentage. In the literature, a majority of studies analyzing stylolite roughness use the Fourier Power Spectrum or the Average Wavelet Coefficient signal analyses (e.g. Karcz and Scholz, 2003; Renard et al., 2004; Schmittbuhl et al., 2004; Ebner et al., 2009a, 2009b; Rolland et al., 2014; Beaudoin et al., 2016;

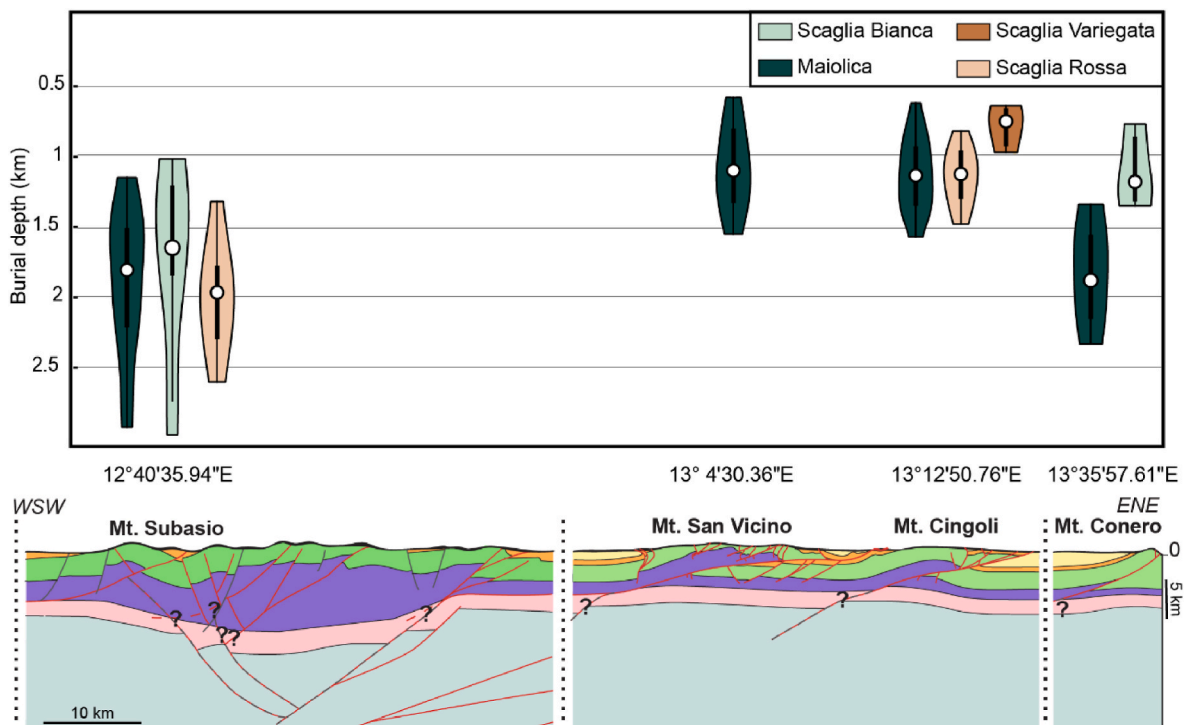


Fig. 7. Distribution of the burial depth derived from L_c values for each studied fold and with respect to the formations. The distributions are represented as box-and-whiskers plots (black boxes limited by the first and third quartile, white circle is the value of the average) included in the corresponding violin plot, as a function of the average longitude of the host structure, represented below on the cross section (see Fig. 2).

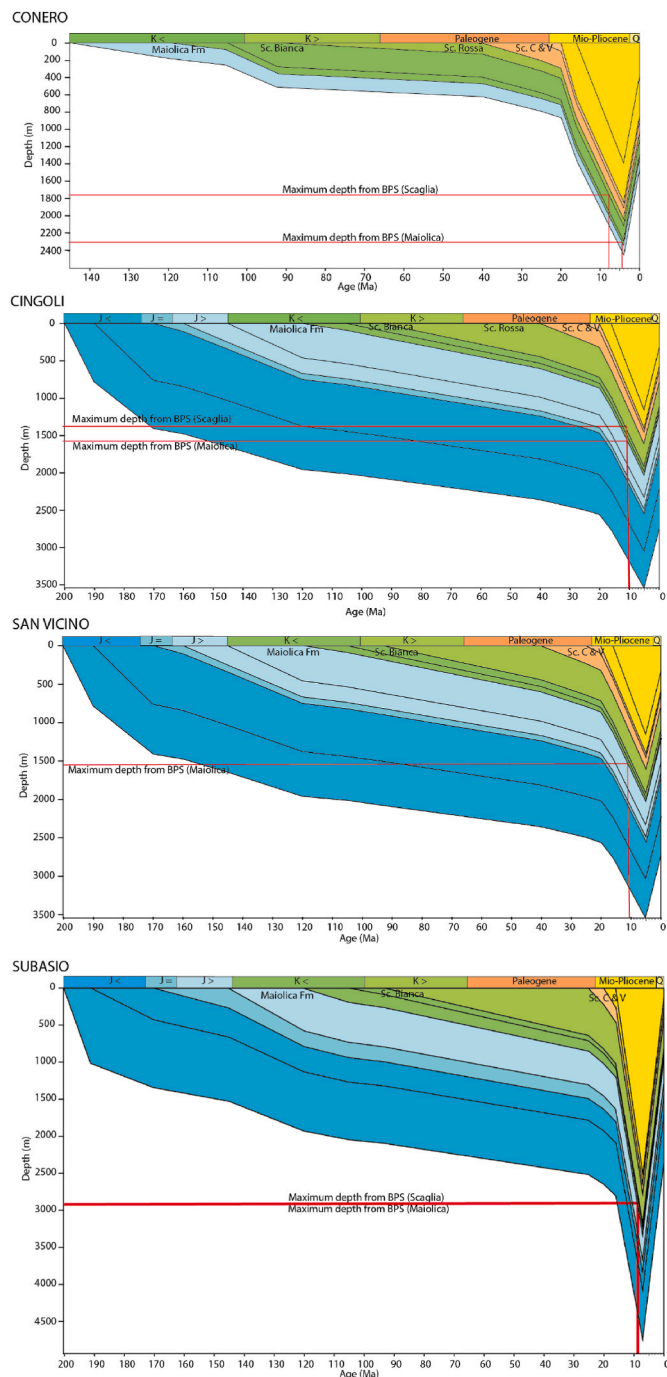


Fig. 8. Burial-time models resulting from the protocol described in the text, with the input values reported in Table S2. The models correspond to, from top to bottom, the Conero Anticline, the Cingoli Anticline, the San Vicino Anticline, and the Subasio Anticline. Dash red lines correspond to the minimum depth at which the shallowest stylolite stopped developing. Solid red lines correspond to the maximum burial depth and the corresponding age at which development of BPS stopped for a given formation. (For interpretation of the references to color in this figure legend, the reader is referred to the Web version of this article.)

Bertotti et al., 2017; Beaudoin et al., 2020c), so we exemplify the consistency criterion using these methods, set by defining the parameter Δ as $\Delta = \frac{LC_{(FPS)} - LC_{(AWC)}}{LC_{(FPS)}}$, if $LC_{(FPS)} > LC_{(AWC)}$. It is noteworthy that this criterion can be extended to include other signal analysis methods that have been proven successful for SRIT, such as the Root Mean Square, the Maximum-Minimum height difference, the Correlation Function, or the RMS Correction function (see Candela et al., 2010; Rolland et al., 2014).

As illustrated on Fig. 5, some valid inversion can return significantly different Lc values according to the signal analysis method used. Overall, in the population of the 157 valid inversions, only 34% of the dataset meet this consistency criterion (Fig. 6B).

The reliability of SRIT improves significantly when proceeding to the inversion of the roughness of the virtual composite stylolite that is made up by linking all stylolites that have the same morphology and are found in the same hand sample. Creating a composite stylolite by concatenating selected stylolite tracks (from 2 to 16 in this case) increases the range of roughness that is sampled during the signal analysis. Our dataset allowed to create 56 composite stylolites (Table S5), and the distribution of the results obtained on composite stylolite is narrower than on single tracks regardless the signal analysis method (Fig. 6C). Using inversion of the roughness of composite stylolite returns more valid inversions (98% for the FPS and 95% for the AWC) and more cases where the inversion is consistent (66% of the dataset, Fig. 6D). This significant improvement strongly suggests that the limited range of available roughness on the studied track of a single stylolite may prevent the roughness inversion to return a consistent value. However, Fig. 6C illustrates that the statistical distribution of the Lc values from a representative population remains similar (within the methodological uncertainty) whether one considers the valid inversion on composite tracks or on single tracks. This means that using a single signal analysis method on a large population of stylolites will provide reliable results in terms of Lc values. It is interesting to note that recent investigations on scaling of stylolite roughness on long tracks (>10 cm) highlighted another change in the scaling regime at the large scale, termed by Koehn et al. (2022) as the correlation length. Above the correlation length, the stylolite amplitude remains constant, and this length was proposed as a proxy to estimate compaction. In concatenated stylolites, such a scaling behavior of the roughness is not observed, supporting that the addition of different stylolites only increases the sample size for the signal analysis, without creating a signal of which amplitude becomes constant at large scale.

Consequently, we recommend to future users to either increase the population of studied stylolites to a statistically significant number (ca. >50) and to apply SRIT with the best suited method of choice, or in case there is not enough data, to conduct the concatenation process to create obviously fewer composite stylolites but the roughness inversion of which will return more reliable and consistent Lc values. An alternative approach that would theoretically provide similar results than concatenation, consists in applying the SRIT process on a binned signal coming from averaging the signal analysis of numerous stylolite tracks in the same sample.

It is also worth noting that the distribution of the Lc values from the studied population differs slightly when considering type 2 (seismogram pinning) stylolites apart from type 3 (suture and sharp peak) stylolites (Fig. 6A). Indeed, the inversion of the roughness of a subpopulation of type 2 stylolites shows a bimodal distribution of Lc values (the corresponding violin envelope has two bumps) while type 3 shows a unimodal distribution (the corresponding violin envelope has one bump). Both types share the same modal value of Lc (0.3–0.5 mm), but the second mode found only considering type 2 stylolite is higher (Lc = 0.9–1.3 mm). If considering the extreme teeth of type 2 do not disturb the signal analysis, type 2 stylolites would correspond to lower magnitudes of the vertical stress at which pressure solution was active, hence, to lower burial depths. Regardless the physical reason for this behavior of type 2 roughness analysis (i.e. intrinsic to stylolite development, or induced by signal analysis disturbance), similar observations were made in other case studies (Beaudoin et al., 2019, 2020a, b, c; Bah et al., 2023), which suggests that the best suited BPS to consider for finding the maximum burial depth experienced by the rock while pressure solution along horizontal planes was active belong to the type 3 BPS. We hence suggest focusing on the type 3 stylolites.

6.2. Geological implications

6.2.1. Dependency of SRIT on rock physics

An important point to stress out is the dependence of the calculated vertical stress values on the mechanical and chemical parameters that are involved in equations (1) and (2). While the solid-fluid interfacial energy is rather well constrained from experiments (Wright et al., 2001), the elastic parameters are hard to quantify as they were at the time pressure solution was active and stopped around the stylolite. The natural variability of the Poisson's ratio in carbonates is rather low (0.18–0.35), and this uncertainty impact on the calculation of the stress is about 10% for extreme values. However, the Young modulus (E) has a much bigger impact, naturally varying in carbonates from 5 GPa to 100 GPa (Hadi and Nygaard, 2023) namely according to porosity. Yet, if it is possible that the effect of pressure solution itself over the elastic properties of carbonates is limited (Wingender et al., 2021), the redistribution of dissolved material in the surrounding pores will likely increase the value of E with time. Also, it was demonstrated that the value of the E increases with applied stress (Pimienta et al., 2015), so it is likely the measurement of E in outcrops underestimates the value of E at the time pressure solution occurred. It is also a matter of debate to use a bulk measurement of E for representing the grain-fluid-grain interface pressure-solution occurs along. There have been several different methods proposed to reconstruct E for the case of SRIT. For instance, one can derive a unique value of E using a population of BPS along a vertical profile (Ebner et al., 2009b), alternatively, SRIT has been used in a case where expected depth was well constrained to show a quantitative evolution of E during stylolite development (Rolland et al., 2014). Other studies rather use the measured value of E derived from triaxial tests on homogeneous material (Beaudoin et al., 2019) or derived from field-scale measurements by Schmidt Hammer (Labeur et al., 2021). In all cases, a variation of +100% in the E value results in a variation of +50% of the calculated vertical stress magnitude (Beaudoin et al., 2016). Because this issue is very impactful on the individual results, we tested the effect of such variation at the scale of the BPS population (Fig. S2). On Fig. 7 the Young moduli used to calculate the vertical stresses and associated burial depths are those determined by the rebound method from field data, established for all studied formations and in each anticline (Table S3). On Fig. S2, the Young moduli correspond to 23 GPa, a value given by Beaudoin et al. (2016) considering a mechanically homogeneous carbonate reservoir. If considering the median value of the distribution, the difference between the calculated depths with an average E or with a locally measured E is below 20% in all cases, suggesting at first order that the distribution of the vertical stress and depth among a studied population is not dramatically affected by the uncertainty on E. It is a complicated topic to discuss the evolution of the elastic parameters of a rock undergoing diagenesis, and more specifically if the E value in the laboratory is a good representative of the E at the pressure conditions at which deformation occurs (e.g. Pimienta et al., 2015), and consequently which value of E is to be used for each given strata. However, we suggest conducting SRIT using, when possible, the value of E calculated from stress-strain plots obtained from rock mechanical tests under a triaxial press applied to homogeneous, undeformed portions of the studied rock, because it should return the highest value of E, consequently the closest to the one prevailing at the time the deepest stylolite stopped developing.

6.2.2. Lessons learned on stylolite development during burial

At first order, the maximum burial depths at which compaction-related pressure solution was active along BPS are consistent at the scale of the individual fold and at the scale of the entire UMAR (Fig. 7), falling in the range 0.5–3 km range and never exceeding the maximum burial depth of the formations hosting the BPS as reconstructed using burial modeling (Fig. 8). In each fold, the highest 75% of the depths obtained from SRIT correspond to the period of increase of the burial rate associated with the fast sedimentation during local flexure. The

possible reason(s) why stylolite development can halt massively (i.e. for most individuals in a population) can be numerous: (i) a saturation effect at the stylolite plane scale related to the depth of deformation (Toussaint et al., 2018); (ii) the clogging of the porosity due to dissolved material reprecipitation that prevents further development of the stylolite plane (Hou et al., 2023); or (iii) the switch of the maximum principal stress from a vertical to a horizontal attitude in response to prevailing tectonic forces (e.g. Peacock et al., 2017b; Beaudoin et al., 2020c); (iv) alternatively a local fluid migration in the reservoir could locally create overpressure around a stylolite/at the grain-fluid interface, inhibiting its development (e.g. Peacock et al., 2017a), with a potential effect on different layers affecting then the whole reservoir (as tentatively proposed to explain a sudden stop in stylolite development during burial concomitant to hydrocarbon migration in pre-salt formation of the lower Congo basin; Bah et al., 2023). To differentiate between these causes is impossible in our case, yet the covality between the halt of activity of most of the studied stylolites and the increase in burial rate suggests that pressure solution could be the most effective way to accommodate vertical shortening up to a certain point, especially once at depth where physical grain reordering is limited, while fluid-rock interactions become more potent. It is worth noting that similar observations that most stylolites would halt during periods of fast burial rates were made in cores from offshore Congo (Bah et al., 2023; Zeboudj et al., 2023).

6.2.3. Regional validation: estimates of the timing of the onset of orogenic stress loading related to apenninic contraction

As previously demonstrated, SRIT applied to a population of sedimentary stylolites is a powerful tool to estimate the first order maximum paleodepth experienced by the strata under a vertical maximum principal stress. In the present case, the reconstructed maximum paleodepth of active pressure solution is lower than the maximum burial depth predicted by the models, which is consistent with the onset of orogenic stress loading during continuing burial of strata; in other words, the maximum principal stress σ_1 did not remain vertical up to the maximum burial depth of strata. When projecting the depth distribution obtained from SRIT applied on BPS collected in the Maiolica and Scaglia Fms onto the burial-time model for each fold, it is possible to estimate the timing when BPS halted. In the Subasio Anticline, such stop of pressure solution development seems to have occurred ca. 9 Ma ago, while it was ca. 10 Ma ago in both the San Vicino and Cingoli anticlines. In the Conero Anticline, this method dates this halt to ca. 4.5 Ma ago. This method was used as a proxy to estimate the very beginning of tectonic contraction in various orogenic forelands (Beaudoin et al., 2019, 2020b, 2021; Labeur et al., 2021; Lacombe et al., 2021). Here, we tentatively compare the timing at which BPS stopped developing to the independently reconstructed timing of fold development (Fig. 9), constrained either by the age of growth strata (Calamita et al., 1994; Mazzoli et al., 2002), or by U–Pb geochronology of syn-kinematic calcite mineralization in tectonic veins and faults (Beaudoin et al., 2020a, b; Lacombe et al., 2021), or both (see general discussion in Lacombe and Beaudoin, 2024). For each individual fold, the reconstructed time at which pressure solution along BPS stopped being active predates the time of fold development at the same place by ca. 3 My. Consequently, when integrating this timing at the scale of the UMAR, we document an eastward sequence of ending compaction-related stylolitization, which is consistent with, and older by 1–4 My than, the reconstructed sequence of younging eastward folding and thrusting (Tavani et al., 2021). The consistently younging eastward sequence of the end of stylolitization and folding throughout the belt validate SRIT as a reliable tool to constrain the timing of the very onset of orogenic stress loading in fold-and-thrust belts and associated foreland domains. These 1–5 My gaps also are locally the maximum duration of the LPS, that might be even shorter if one considers a transient period of progressively increasing tectonic stress loading until the stress level needed to initiate LPS is reached. This short duration is in line with previous studies based on U–Pb dating of syn-kinematic calcite mineralization from tectonic veins that suggested that the duration of

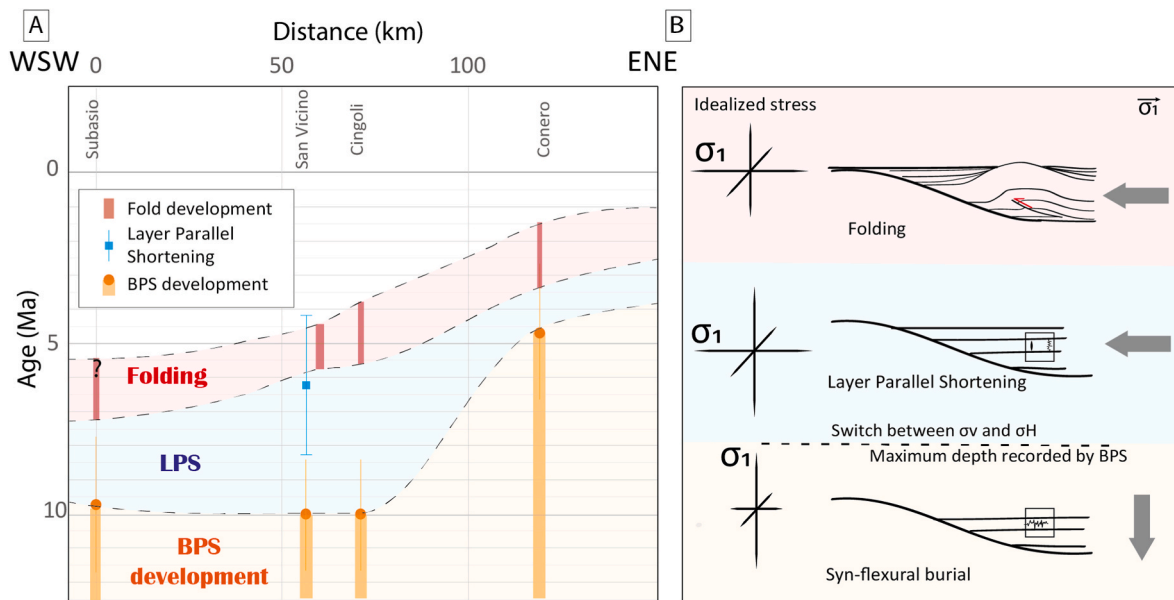


Fig. 9. (A) Plot of age of burial/tectonic history (in Ma) vs eastward current distance from the Subasio Anticline (km). In orange are reported the end period of the BPS development as calculated from SRIT in the present study. In blue is reported the only available absolute age (U–Pb) of synkinematic calcite mineralization related to layer-parallel shortening (Lacombe et al., 2021), and in red are reported the duration of the folding events as estimated from the age of growth strata (Calamita et al., 1994; Mazzoli et al., 2002). (B) Sketches idealizing the evolution of the strata corresponding to the three phases highlighted in (A), with an emphasis on the corresponding conceptual relative stress orientation and magnitude, and on the mesostructures developing in the strata during this history. (For interpretation of the references to color in this figure legend, the reader is referred to the Web version of this article.)

the LPS may be as short as 1 My (Lacombe et al., 2021; Lacombe and Beaudoin, 2024). The results based on SRIT across the belt strengthen the model of rapid propagation of the deformation and quick sequence of activation of décollement level that developed folds in the UMAR, mitigating a tectonic model where the UMAR developed by thick-skinned tectonics and inversion of basement faults only.

7. Conclusions

The goal of this study applied to the Umbria Marche Apennine Ridge was to confidently and critically assess the best way to conduct SRIT so that the inversion reliably yields the paleodepths experienced by carbonate strata at the time pressure solution mechanism was efficient to accommodate burial related compaction. We define two criteria to assess the quality of the inversion results: the *validity*, reached when the signal treatment of the 1D profile returns two well-defined slopes of auto-affine behavior that are consistent with the Hurst exponents predicted by Schmittbuhl et al. (2004); and the *consistency*, reached when two signal analysis methods (FPS and AWC) return the same Lc value within intrinsic uncertainty (23%). We show that the discrepancy between the Lc returned by FPS and AWC applied on the same track in >75% of cases is likely related to the limited sampling of the roughness along a stylolite track. Indeed, by conducting SRIT on composite stylolites, created by concatenating numerous stylolites of the same morphology found in the same rock, the SRIT returns a better consistency in the results, while not changing the Lc value of stylolites of which inversion is valid.

The study of a large-scale population of sedimentary stylolites teaches us that while the selected values of the Young modulus have a massive impact on the uncertainty of the SRIT (up to 50% for 100% variation of the E value), this impact is mitigated when considering the distribution of Lc obtained from a large population of stylolites, i.e. the values of quartiles and medians are impacted by less than 20%. Using the distribution of depths at which pressure-solution was active as derived from the Lc values of the population of sedimentary stylolites in combination with burial-time models to constrain the timing of stylolite development under a vertical σ_1 , e.g., during compaction with negligible

horizontal stress, is a powerful tool when studying the structural evolution of an area. To validate this approach, we considered the calendar of halting of the sedimentary stylolite development in four folds across the UMAR. This calendar shows an eastward sequence consistent with the recorded sequence of folding across the UMAR, with a time gap of 1–5 My between the end of BPS development and the oldest age of growth strata in each fold. The consistency between the timing and sequence of the halt of BPS development on the one hand and the timing of folding given by absolute dating of either synfolding strata or fold-related fractures on the other hand, is a strong support to using SRIT applied to BPS in fold-and-thrust belts to assess the timing of when the tectonic-related horizontal σ_1 has increased enough to overcome the burial-related vertical stress, triggering first layer parallel shortening, then later folding and thrusting.

CRediT authorship contribution statement

Aurélien Labeur: Conceptualization, Data curation, Formal analysis, Investigation, Methodology, Writing – original draft. **Nicolas E. Beaudoin:** Conceptualization, Data curation, Formal analysis, Funding acquisition, Investigation, Methodology, Project administration, Resources, Software, Supervision, Validation, Writing – original draft, Writing – review & editing. **Olivier Lacombe:** Conceptualization, Supervision, Writing – original draft, Writing – review & editing. **Claude Gout:** Formal analysis, Software, Writing – original draft. **Jean-Paul Callot:** Conceptualization, Supervision, Writing – review & editing.

Declaration of competing interest

The authors declare that they have no known competing financial interests or personal relationships that could have appeared to influence the work reported in this paper.

Data availability

Data will be made available on request.

Acknowledgement

A.L. and N.E.B are funded through the ISITE programme E2S, supported by ANR PIA and Région Nouvelle-Aquitaine. The PhD of A.L. benefited from the extra-support of TotalEnergies. Beicip-Franlab is acknowledged for providing licences of the basin simulator TemisFlow™.

Appendix A. Supplementary data

Supplementary data to this article can be found online at <https://doi.org/10.1016/j.jsg.2024.105098>.

References

- Alvarez, W., 1989. Evolution of the Monte nerone seamount in the umbria-marche apennines: II. Tectonic control of the seamount-basin transition. *Boll. Soc. Geol. Ital.* 108, 23–39.
- Alvarez, W., Arthur, M.A., Fischer, A.G., Lowrie, W., Napoleone, G., Silva, I.P., Roggenthen, W.M., 1977. Upper Cretaceous-Paleocene magnetic stratigraphy at Gubbio, Italy: V. Type section for the Late Cretaceous-Paleocene geomagnetic reversal time scale. *Geol. Soc. Am. Bull.* 88, 383–389.
- Alvarez, W., Engelder, T., Geiser, P.A., 1978. Classification of solution cleavage in pelagic limestones. *Geology* 6 (5), 263–266.
- Atashbari, V., Tingay, M., 2012. Pore pressure prediction in carbonate reservoirs. In: SPE Latin America and Caribbean Petroleum Engineering Conference. OnePetro Conference. April 2012.
- Aydin, A., Basu, A., 2005. The Schmidt hammer in rock material characterization. *Engineering Geology* 81, 1–14.
- Bah, B., Beaudoin, N.E., Lacombe, O., Girard, J.-P.P., Gout, C., Godeau, N., Deschamps, P., 2023. Multi-proxy reconstruction of the burial history and porosity evolution of the TOCA carbonate formation in the Lower Congo Basin (South West Africa). *Mar. Petrol. Geol.* 148, 106018.
- Bally, A.W., Burbi, W., Cooper, J.C., Ghelardoni, L., 1986. Balanced Sections and Seismic Reflection Profiles across the Central Apennines, Italy, vol. 77. Memoir Society Geological Italy, pp. 63–78.
- Barabási, A.L., Stanley, H.E., 1995. *Fractal Concepts in Surface Growth*. Cambridge university press.
- Barchi, M.R., Alvarez, W., Shimabukuro, D.H., 2012. The Umbria-Marche Apennines as a double orogen: observations and hypotheses. *Italian Journal of Geosciences* 131, 258–271.
- Barchi, M.R., Tavarnelli, E., 2022. Thin vs. thick-skinned tectonics in the Umbria-Marche fold-and-thrust belt: contrast or coexistence? In: Koerber, C., Claeys, P., Montarini, A. (Eds.), *From the Guajira Desert to the Apennines, and from Mediterranean Microplates to the Mexican Killer Asteroid: Honoring the Career of Walter Alvarez*. GSA Special Papers, p. 557.
- Beaudoin, N., Gasparrini, M., David, M.-E., Lacombe, O., Koehn, D., 2019. Bedding-parallel stylolites as a tool to unravel maximum burial depth in sedimentary basins: application to Middle Jurassic carbonate reservoirs in the Paris basin, France. *GSA Bulletin* 131, 1239–1254.
- Beaudoin, N., Koehn, D., Lacombe, O., Lecouty, A., Billi, A., Aharonov, E., Parlangeau, C., 2016. Fingerprinting stress: stylolite and calcite twinning paleopiezometry revealing the complexity of progressive stress patterns during folding—the case of the Monte Nero anticline in the Apennines, Italy. *Tectonics* 35, 1687–1712.
- Beaudoin, N., Labeur, A., Lacombe, O., Koehn, D., Billi, A., Hoareau, G., Boyce, A., John, C.M., Marchegiano, M., Roberts, N.M., Millar, I.L., Clavierie, F., Pecheyran, C., Callot, J.-P., 2020a. Regional-scale paleofluid system across the Tuscan Nappe – Umbria Marche Arcuate Ridge (northern Apennines) as revealed by mesostructural and isotopic analyses of stylolite-vein networks. *Solid Earth* 11, 1617–1641. <https://doi.org/10.5194/se-11-1617-2020>.
- Beaudoin, N., Lacombe, O., 2018. Recent and future trends in paleopiezometry in the diagenetic domain: insights into the tectonic paleostress and burial depth history of fold-and-thrust belts and sedimentary basins. *J. Struct. Geol.* 114, 357–365.
- Beaudoin, N., Lacombe, O., David, M., Koehn, D., 2020b. Does stress transmission in forelands depend on structural style? Distinctive stress magnitudes during Sevier thin-skinned and Laramide thick-skinned layer-parallel shortening in the Bighorn Basin (USA) revealed by stylolite and calcite twinning paleopiez. *Terra. Nova* 32, 225–233.
- Beaudoin, N., Lacombe, O., Koehn, D., David, M.-E., Farrell, N., Healy, D., 2020c. Vertical stress history and paleoburial in foreland basins unravelled by stylolite roughness paleopiezometry: insights from bedding-parallel stylolites in the Bighorn Basin, Wyoming, USA. *J. Struct. Geol.* 136, 104061.
- Ben-Itzhak, L.L., Aharonov, E., Toussaint, R., Sagy, A., 2012. Upper bound on stylolite roughness as indicator for amount of dissolution. *Earth Planet Sci. Lett.* 337, 186–196.
- Bertotti, G., de Graaf, S., Bisdom, K., Oskam, B., Vonhof, H.B., Bezerra, F.H., Reijmer, J.J.G., Cazarin, C.L., 2017. Fracturing and fluid-flow during post-rift subsidence in carbonates of the Jandaíra Formation, Potiguar Basin, NE Brazil. *Basin Res.* 29 (6), 836–853.
- Bigi, S., Milli, S., Corrado, S., Casero, P., Aldega, L., Botti, F., Moscatelli, M., Stanzione, O., Falcini, F., Marini, M., 2009. Stratigraphy, structural setting and burial history of the Messinian Laga basin in the context of Apennine foreland basin system. *Journal of Mediterranean Earth Sciences* 1, 61–84.
- Boccaletti, M., Calamita, F., Viandante, M.G., 2005. The lithospheric apennine neo-chain developing since the lower Pliocene as a result of the africa-europe convergence. *Boll. Soc. Geol. Ital.* 124, 87–105.
- Brozzetti, F., Cirillo, D., Luchetti, L., 2021. Timing of contractional tectonics in the Miocene foreland basin system of the Umbria pre-apennines (Italy): an updated overview. *Geosciences* 11, 97.
- Calamita, F., Cello, G., Deiana, G., Paltrinieri, W., 1994. Structural styles, chronology rates of deformation, and time-space relationships in the Umbria-Marche thrust system (central Apennines, Italy). *Tectonics* 13, 873–881.
- Calamita, F., Deiana, G., 1988. The arcuate shape of the Umbria-Marche-Sabina Apennines (central Italy). *Tectonophysics* 146, 139–147.
- Calamita, F., Paltrinieri, W., Pelorosso, M., Scisciani, V., Tavarnelli, E., 2003. Inherited Mesozoic architecture of the Adria continental palaeomargin in the neogene central apennines orogenic system, Italy. *Boll. Soc. Geol. Ital.* 122, 307–318.
- Candela, T., Renard, F., Bouchon, M., Brouste, A., Marsan, D., Schmittbuhl, J., Voisin, C., 2010. Characterization of fault roughness at various scales: implications of three-dimensional high resolution topography measurements. *Pure Appl. Geophys.* 166, 1817–1851.
- Carminati, E., Lustrino, M., Cuffaro, M., Doglioni, C., 2010. Tectonics, magmatism and geodynamics of Italy: what we know and what we imagine. *J. Virtual Explor.* 36, 10–3809.
- Cello, G., Mazzoli, S., Tondi, E., Turco, E., 1997. Active tectonics in the central Apennines and possible implications for seismic hazard analysis in peninsular Italy. *Tectonophysics* 272, 43–68.
- Cipriani, A., Fabbri, S., Lathuilière, B., Santantonio, M., 2019. A reef coral in the condensed Maiolica facies on the Mt Nerone pelagic carbonate platform (Marche Apennines): the enigma of ancient pelagic deposits. *Sediment. Geol.* 385, 45–60.
- Conti, S., Argentino, C., Fioroni, C., Salocchi, A.C., Fontana, D., 2021. Miocene seep-carbonates of the northern apennines (emilia to Umbria, Italy): an overview. *Geosci.* 11, 53, 2021, Vol. 11, Page 53.
- Decandia, F.A., Tavarnelli, E., Alberti, M., 2002. Pressure-solution fabrics and their overprinting relationships within a minor fold train of the Umbria-Marche Apennines, Italy. *Boll. Soc. Geol. Ital.* 1, 687–694.
- Díaz General, E.N., Mollema, P.N., Antonellini, M., 2015. Fracture patterns and fault development in the pelagic limestones of the Monte Conero Anticline (Italy). *Ital. J. Geosci.* 134, 495–512.
- Ebner, M., Koehn, D., Toussaint, R., Renard, F., 2009a. The influence of rock heterogeneity on the scaling properties of simulated and natural stylolites. *J. Struct. Geol.* 31, 72–82.
- Ebner, M., Koehn, D., Toussaint, R., Renard, F., Schmittbuhl, J., 2009b. Stress sensitivity of stylolite morphology. *Earth Planet Sci. Lett.* 277, 394–398.
- Ebner, M.J., 2009. *The Development of Stylolites, from Small-Scale Heterogeneities to Multi-Scale Roughness*. Mainz University, Germany. PhD thesis.
- Elter, F.M., Elter, P., Eva, C., Eva, E., Kraus, R.K., Padovano, M., Solarino, S., 2012. An alternative model for the recent evolution of the Northern–Central Apennines (Italy). *J. Geodyn.* 54, 55–63.
- Fancelli, R., Radrizzani, S., 1964a. Geological Map of Italy, Ancona, Sheet 118.
- Fancelli, R., Radrizzani, S., 1964b. Note Illustrative della Carta Geologica d'Italia alla scala 1:100.000, Foglio 118, Ancona. Ministero dell'Industria e del Commercio, Direzione Generale delle Miniere. Servizio Geologico d'Italia. Libreria dello Stato, Roma.
- Ghisetti, F., Vezzani, L., 2002. Normal faulting, extension and uplift in the outer thrust belt of the central Apennines (Italy): role of the Caramanico fault. *Basin Res.* 14, 225–236.
- Guerrera, F., Tramontana, M., Donatelli, U., Serrano, F., 2012. Space/time tectono-sedimentary evolution of the umbria-romagna-marche Miocene basin (northern apennines, Italy): a foredeep model. *Swiss J. Geosci.* 105, 325–341.
- Hadi, F., Nygaard, R., 2023. Estimating unconfined compressive strength and Young's modulus of carbonate rocks from petrophysical properties. *Petrol. Sci. Technol.* 41 (13), 1367–1389.
- Hintze, J.L., Nelson, R.D., 1998. Violin plots: a box plot-density trace synergism. *Am. Statistician* 52, 181–184.
- Hippolyte, J.-C., Angelier, J., Barrier, E., 1995. Compressional and extensional tectonics in an arc system: example of the Southern Apennines. *J. Struct. Geol.* 17, 1725, 170.
- Hou, Z., Fusses, F., Schöpfer, M., Grasemann, B., 2023. Synkinematic evolution of stylolite porosity. *J. Struct. Geol.* 173, 104916.
- Karcz, Z., Scholz, C.H., 2003. The fractal geometry of some stylolites from the Calcare Massiccio Formation, Italy. *J. Struct. Geol.* 25, 1301–1316.
- Katz, O., Reches, Z., Roegiers, J.-C., 2000. Evaluation of mechanical rock properties using a Schmidt Hammer. *Int. J. Rock Mech. Min. Sci.* 37, 723–728.
- Koehn, D., Ebner, M., Renard, F., Toussaint, R., Passchier, C.W., 2012. Modelling of stylolite geometries and stress scaling. *Earth Planet Sci. Lett.* 341, 104–113.
- Koehn, D., Köehler, S., Toussaint, R., Ghani, I., Stollhofen, H., 2022. Scaling analysis, correlation length and compaction estimates of natural and simulated stylolites. *J. Struct. Geol.* 161, 104670.
- Koehn, D., Renard, F., Toussaint, R., Passchier, C.W., 2007. Growth of stylolite teeth patterns depending on normal stress and finite compaction. *Earth Planet Sci. Lett.* 257, 582–595.
- Koehn, D., Rood, M.P., Beaudoin, N., Chung, P., Bons, P.D., Gomez-Rivas, E., 2016. A new stylolite classification scheme to estimate compaction and local permeability variations. *Sediment. Geol.* 346, 60–71.
- Labeur, A., Beaudoin, N.E., Lacombe, O., Emmanuel, L., Petracchini, L., Daéron, M., Klimowicz, S., Callot, J.-P., 2021. Burial-deformation history of folded rocks unraveled by fracture analysis, stylolite paleopiezometry and vein cement

- geochemistry: a case study in the Cingoli Anticline (Umbria-Marche, northern Apennines). *Geosciences* 11, 135.
- Lacombe, O., Beaudoin, N., Hoareau, G., Labeur, A., Pecheyran, C., Callot, J.-P., 2021. Dating folding beyond folding, from layer-parallel shortening to fold tightening, using mesostructures: lessons from the Apennines, Pyrenees and Rocky Mountains. *Solid Earth* 12, 2145–2157. <https://doi.org/10.5194/se-12-2145-2021>.
- Lacombe, O., Bellahsen, N., 2016. Thick-skinned tectonics and basement-involved fold-thrust belts: insights from selected Cenozoic orogens. *Geol. Mag.* 153, 763–810.
- Lacombe, O., Beaudoin, N.E., 2024. Timing, sequence, duration and rate of deformation in fold-and-thrust belts: a review of traditional approaches and recent advances from absolute dating (K-Ar illite/U-Pb calcite) of brittle structures. *Compt. Rendus Geosci.* 356, S2. <https://doi.org/10.5802/crgeos.218>.
- Lavecchia, G., Minelli, G., Piali, G., 1988. The Umbria-Marche arcuate fold belt (Italy). *Tectonophysics* 146, 125–137.
- Marshak, S., Geiser, P.A., Alvarez, W., Engelder, T., 1982. Mesoscopic fault array of the northern Umbrian Apennine fold belt, Italy: geometry of conjugate shear by pressure-solution slip. *Geol. Soc. Am. Bull.* 93, 1013–1022.
- Mazzoli, S., Aldega, L., Corrado, S., Invernizzi, C., Zattin, M., 2006. Pliocene-quaternary thrusting, syn-orogenic extension and tectonic exhumation in the Southern Apennines (Italy): insights from the Monte Alpi area. In: Mazzoli, S., Butler, R.W.H. (Eds.), *Styles of Continental Contraction, GSA Special Paper*, vol. 414, p. 55.
- Mazzoli, S., Cello, G., Deiana, G., Galdenzi, S., Gambini, R., Mancinelli, A., Mattioni, L., Shiner, P., Tondi, E., 2000. Modes of foreland deformation ahead of the Apennine thrust front. *J. Czech Geol. Soc.* 45, 246.
- Mazzoli, S., Deiana, G., Galdenzi, S., Cello, G., 2002. Miocene fault-controlled sedimentation and thrust propagation in the previously faulted external zones of the Umbria-Marche Apennines, Italy. *EGU Stephan Mueller Spec. Publ. Ser.* 1, 195–209.
- Naeser, N.D., McCulloch, T.H. (Eds.), 2012. *Thermal History of Sedimentary Basins: Methods and Case Histories*. Springer Science & Business Media.
- Pace, P., Calamita, F., 2014. Push-up inversion structures v. fault-bend reactivation anticlines along oblique thrust ramps: examples from the Apennines fold-and-thrust belt (Italy). *J. Geol. Soc. London* 171, 227–238.
- Pace, P., Pasqui, V., Tavarnelli, E., Calamita, F., 2017. Foreland-directed gravitational collapse along curved thrust fronts: insights from a minor thrust-related shear zone in the Umbria-Marche belt, central-northern Italy. *Geol. Mag.* 154 (2), 381–392.
- Pace, P., Calamita, F., Tavarnelli, E., 2022. Shear zone fabrics and their significance in curved, inverted basin-derived thrust systems. *J. Struct. Geol.* 161, 104663.
- Peacock, D.C.P., Anderson, M.W., Rotevatn, A., Sanderson, D.J., Tavarnelli, E., 2017a. The interdisciplinary use of "overpressure". *J. Volcanol. Geoth. Res.* 341, 1–5.
- Peacock, D.C.P., Tavarnelli, E., Anderson, M.W., 2017b. The interplay between stress permutations and overpressure to cause strike-slip faulting during tectonic inversion. *Terra. Nova* 29, 61–70.
- Perrier, R., Quiblier, J., 1974. Thickness changes in sedimentary layers during compaction history; methods for quantitative evaluation. *AAPG Bull.* 58 (3), 507–520.
- Petracchini, L., Antonellini, M., Billi, A., Scrocca, D., 2012. Fault development through fractured pelagic carbonates of the Cingoli anticline, Italy: possible analog for subsurface fluid-conductive fractures. *J. Struct. Geol.* 45, 21–37.
- Pimienta, L., Fortin, J., Guéguen, Y., 2015. Experimental study of Young's modulus dispersion and attenuation in fully saturated sandstones. *Geophysics* 80 (5), L57–L72.
- Regnet, J.B., David, C., Robion, P., Menéndez, B., 2019. Microstructures and physical properties in carbonate rocks: a comprehensive review. *Mar. Petrol. Geol.* 103, 366–376.
- Renard, F., Schmittbuhl, J., Gratier, J.P., Meakin, P., Merino, E., 2004. Three-dimensional roughness of stylolites in limestones. *Journal of Geophysical Research* 109, B03209. <https://doi.org/10.1029/2003jb002555>.
- Rolland, A., Toussaint, R., Baud, P., Conil, N., Landrein, P., 2014. Morphological analysis of stylolites for paleostress estimation in limestones. *Int. J. Rock Mech. Min. Sci.* 67, 212–225.
- Rolland, A., Toussaint, R., Baud, P., Schmittbuhl, J., Conil, N., Koehn, D., Renard, F., Gratier, J., 2012. Modeling the growth of stylolites in sedimentary rocks. *J. Geophys. Res.* 117, B06403.
- Roure, F., Andriessen, P., Callot, J.P., Faure, J.L., Ferket, H., Gonzales, E., Guilhaumou, N., Lacombe, O., Malandain, J., Sassi, W., Schneider, F., Swennen, R., Vilasi, N., 2010. The use of palaeo-thermo-barometers and coupled thermal, fluid flow and pore-fluid pressure modelling for hydrocarbon and reservoir prediction in fold and thrust belts. *Geological Society* 348 (1), 87–114. London, Special Publications.
- Rusciadelli, G., Viandante, M.G., Calamita, F., Cook, A.C., 2005. Burial-exhumation history of the central Apennines (Italy), from the foreland to the chain building: thermochronological and geological data. *Terra. Nova* 17, 560–572.
- Sabbatino, M., Tavani, S., Vitale, S., Ogata, K., Corradetti, A., Consorti, L., Arienzo, I., Cipriani, A., Parente, M., 2021. Forebulge migration in the foreland basin system of the central-southern Apennine fold-thrust belt (Italy): new high-resolution Sr-isotope dating constraints. *Basin Res.* 33, 2817–2836.
- Sachpazis, C.I., 1990. Correlating Schmidt hardness with compressive strength and Young's modulus of carbonate rocks. *Bull. Eng. Geol. Environ.* 42 (1), 75–83.
- Santantonio, M., 1993. Facies associations and evolution of pelagic carbonate platform/basin systems: examples from the Italian Jurassic. *Sedimentology* 40, 1039–1067.
- Satolli, S., Pace, P., Viandante, M.G., Calamita, F., 2014. Lateral variations in tectonic style across cross-strike discontinuities: an example from the Central Apennines belt (Italy). *Int. J. Earth Sci.* 103, 2301–2313.
- Schmittbuhl, J., Renard, F., Gratier, J.-P.P., Toussaint, R., 2004. Roughness of stylolites: implications of 3D high resolution topography measurements. *Phys. Rev. Lett.* 93, 238501.
- Scisciani, V., Agostini, S., Calamita, F., Pace, P., Cilli, A., Giori, I., Paltrinieri, W., 2014. Positive inversion tectonics in foreland fold-and-thrust belts: a reappraisal of the Umbria-Marche Northern Apennines (Central Italy) by integrating geological and geophysical data. *Tectonophysics* 530, 211–224.
- Scisciani, V., Calamita, F., Tavarnelli, E., Rusciadelli, G., Ori, G.G., Paltrinieri, W., 2001. Foreland-dipping normal faults in the inner edges of syn-orogenic basins: a case from the Central Apennines, Italy. *Tectonophysics* 330, 211–224.
- Scisciani, V., Montefalcone, R., Mazzoli, S., Butler, R.W.H., 2006. Coexistence of thin- and thick-skinned tectonics: an example from the Central Apennines, Italy. *Spec. Pap. Soc. Am.* 414, 33.
- Simonsen, I., Hansen, A., Nes, O.M., 1998. Determination of the Hurst exponent by use of wavelet transforms. *Phys. Rev.* 58 (3), 2779.
- Storti, F., Rossetti, F., Salvini, F., 2001. Structural architecture and displacement accommodation mechanisms at the termination of the Priestley Fault, northern Victoria Land, Antarctica. *Tectonophysics* 341, 141–161.
- Stockdale, P.B., 1926. The stratigraphic significance of solution in rocks. *J. Geol.* 34 (5), 399–414.
- Tavani, S., Storti, F., Bausa, J., Muñoz, J.A., 2012. Late thrusting extensional collapse at the mountain front of the northern Apennines (Italy). *Tectonics* 31, TC4019.
- Tavani, S., Storti, F., Fernández, O., Muñoz, J.A., Salvini, F., 2006. 3-D deformation pattern analysis and evolution of the Aníscolo anticline, southern Pyrenees. *J. Struct. Geol.* 28, 695–712.
- Tavani, S., Storti, F., Lacombe, O., Corradetti, A., Muñoz, J.A., Mazzoli, S., 2015. A review of deformation pattern templates in foreland basin systems and fold-and-thrust belts: implications for the state of stress in the frontal regions of thrust wedges. *Earth Sci. Rev.* 141, 82–104.
- Tavani, S., Storti, F., Salvini, F., Toscano, C., 2008. Stratigraphic versus structural control on the deformation pattern associated with the evolution of the Mt. Catria anticline, Italy. *J. Struct. Geol.* 30, 664–681.
- Tavani, S., Cardello, G.L., Vignaroli, G., Balsamo, F., Parente, M., Sabbatino, M., Raffi, I., Billi, A., Carminati, E., 2021. Segmentation of the apenninic margin of the tyrrhenian back-arc basin forced by the subduction of an inherited transform system. *Tectonics* 40 (9), e2021TC006770.
- Tavarnelli, E., 1996a. Ancient synsedimentary structural control on thrust ramp development: an example from the Northern Apennines, Italy. *Terra. Nova* 8, 65–74.
- Tavarnelli, E., 1996b. The effects of pre-existing normal faults on thrust ramp development: an example from the Northern Apennines, Italy. *Geol. Rundsch.* 85 (2), 363–371.
- Tavarnelli, E., 1997. Structural evolution of a foreland fold-and-thrust belt: the Umbria-Marche Apennines, Italy. *J. Struct. Geol.* 19, 523–534.
- Tissot, B.P., Pelet, R., Ungerer, P.H., 1987. Thermal history of sedimentary basins, maturation indices, and kinetics of oil and gas generation. *AAPG Bull.* 71 (12), 1445–1466.
- Toussaint, R., Aharonov, E., Koehn, D., Gratier, J.-P., Ebner, M., Baud, P., Rolland, A., Renard, F., 2018. Stylolites: a review. *J. Struct. Geol.* 114, 163–195.
- Tozer, R.S.J., Butler, R.W.H., Corrado, S., 2002. Comparing thin- and thick-skinned thrust tectonic models of the Central Apennines, Italy. *EGU Stephan Mueller Spec. Publ. Ser.* 1, 181–194.
- Wingender, B., Azuma, M., Krywka, C., Zaslansky, P., Boyle, J., Deymier, A., 2021. Carbonate substitution significantly affects the structure and mechanics of carbonated apatites. *Acta Biomater.* 122, 377–386.
- Wright, K., Cygan, R.T., Slater, B., 2001. Structure of the (1014) surface of calcite, dolomite and magnesite under wet and dry conditions. *MRS Online Proc. Libr.* 620, 1–6.
- Yalcin, M.N., Littke, R., Sachsenhofer, R.F., 1997. Thermal history of sedimentary basins. In: *Petroleum and Basin Evolution: Insights from Petroleum Geochemistry, Geology and Basin Modeling*. Springer Berlin Heidelberg, Berlin, Heidelberg, pp. 71–167.
- Zeboudj, A., Bah, B., Lacombe, O., Beaudoin, N., Gout, C., Godeau, N., Girard, J.-P., Deschamps, P., 2023. Depicting past stress history at passive margins: a combination of calcite twinning and stylolite roughness paleoepiezometry in supra-salt Sendji deep carbonates, lower Congo Basin, west Africa. *Mar. Petrol. Geol.* 152, 106219.